LA-UR-17-29064
Approved for public release; distribution is unlimited.

Title: Direct Cast U-6Nb – 2017 Progress on Cylindrical Castings

Author(s): Aikin, Robert M. Jr.

Intended for: Report

Issued: 2017-10-04

LA-UR-17-
September 28, 2017

Direct Cast U-6Nb – 2017 Progress on Cylindrical Castings

Robert M. Aikin Jr.
Sigma Division
Los Alamos National Laboratory
P.O. Box 1663, Los Alamos, NM 87545

Abstract

This report describes work to further develop a sound technical basis and best practices for mold design and process parameters for the Direct Casting of U-6wt%Nb components. One major challenge to the production of U-6Nb components is the propensity for niobium segregation during casting and solidification. This is especially true for cylindrical castings where the vertical side walls allow flotation of Nb resulting in severe inverse macro-segregation. In this work, a small (120 mm diameter by 180 mm tall) and large cylinder (250 mm diameter by 310 mm tall) are examined with a focus on reducing, or eliminating, niobium segregation. It is demonstrated that counter gravity casting (top-to-bottom solidification) can be used to minimize segregation in the small cylinder. Attempts to counter gravity cast the large cylinder were unsuccessful, in large part due to size limitations of the current furnace. A path forward for casting of the large cylinders is discussed.

Table of Contents

1. Introduction

This report summarizes FY'17 casting development work on U-6wt%Nb cylinder shaped castings performed by the LANL Foundry and Solidification Science Team within the Sigma Division. The major focus is on the counter gravity casting methodology that avoids the unwanted macro-segregation of niobium during solidification.

1.1 Segregation in U-Nb Castings

Historically U-6Nb castings have exhibited significant inverse segregation of Nb. For a casting that slowly solidifies, it is observed that the bottom of the casting is low in Nb and the top of the casting is high in Nb. This trend will be evident in the conventionally cast cylinders discussed in section 2. For a casting that solidifies quickly the macro-segregation is less significant.

In Fig. 1 the uranium rich side of uranium-niobium phase diagram [1-2] is shown. Also shown is density for solid and liquid at the melting point versus niobium content]. The density of the liquid was experimentally determined by Drotning [3]. The density of the solid (shown as a dotted line) is estimated from the published pure U density [4] and the assumption that the compositional dependence of the liquid is the same at the dependence determined by Drotning for the solid.

It is believed that inverse segregation in U-Nb castings occurs based on the following mechanism. The phase diagram (Fig. 1) shows that the first solid to form from a U-6Nb liquid cools has a composition of 10wt%Nb. This first solid (F_S), has a density that is lower than the density of the liquid from which it forms (F_L). The density of the first solid is 15.2 g/cm^3, while the density of the liquid is 15.5 g/cm^3. This difference of approximately 2% means that the first solid to form will want to float because of simple buoyancy considerations.

Figure 2 compares two of common solidification morphologies. In the ingot on left, solidification is by columnar grown and the solid grains grow out from the mold wall forming long columnar grains. Here the heat is conducted way from the solid/liquid interface and out through the solid to the mold. As solidification continues the liquid can become constitutionally supercooled and the solidification morphology will transition to equiaxed free dendritic growth [5].

If U-6Nb solidifies by free dendritic growth, then solid can float straight away. If U-6Nb solidifies by columnar growth, then solid can float if dendrite arms or tips breakoff. In either case, solid can find itself in the liquid and the density difference will result in flotation of Nb rich solid. It is believed that this is the mechanism responsible for the inverse segregation observed in slowly cooled U-6Nb castings.

This pattern of macro-segregation is called *inverse segregation* because the phase diagram indicates that the first solid to form is high in niobium, while it is observed is that the first part of the casting to solidify (the bottom) is low in niobium. Since this pattern of

macro-segregation is opposite what the phase diagram would suggest it is termed inverse segregation.

1.2 Counter Gravity Casting

Figure 3 compares two ways to avoid the floatation of Nb rich solid during solidification.

In the case of a conventional uranium casting (on the left). The mold is heated such that there is a positive thermal gradient, with the mold cool at the bottom and hot at the top. The molten metal is poured into the top of the mold. Solidification progresses from mold bottom to top. If the solidification front advancement rate (the solidification rate) is faster than the buoyancy driven floatation of the Nb rich free dendrites (or broken off dendrite tips), then there won't be signification macro-segregation. If the solidification front advancement rate is lower than the buoyancy driven floatation of the Nb rich free dendrites, then the casting will be Nb-lean at the bottom and Nb-rich at the top. This behavior is consistent with the observed inverse macro-segregation observed in slow cooled U-Nb castings.

If the casting is forced to solidify from top to bottom (solidify in a direction counter to gravity), then any Nb rich solid that tries to float will be met by the solidification front moving in the opposite direction. Such a top-to-bottom solicitation pattern can be produced by having a negative thermal gradient in the mold (cool at top and hot at the bottom) and by filling from top to bottom. Such a counter gravity solidification approach has the advantage that it does not depend on the solidification rate. It has the disadvantage that the metal must be pressurized by the casting rigging system during solidification. If it does not remain pressurized, the metal will cavitate and form macro-porosity.

In this work, we will try to develop the techniques that utilize counter gravity casting to produce segregation free U-6Nb cylinder castings.

2. Small 120 mm Diameter Cylinders

In 2009, under the Accelerated Casting Technology Insertion Testworks Program (ACTI-Testworks), a set of conventional top fill 120 mm diameter by 180 mm tall U-6Nb castings were made as a function of casting thickness (8 and 16 mm) and mold temperature at pour time. The intent of these casting experiments was to better understand the relationship between casting temperature, casting thickness, and Nb segregation. The processing conditions were chosen such that the 16 mm thick casting with the regular mold preheat temperature casting would have the same nominal solidification time at the 8 mm thick casting with a hot mold preheat temperature casting. This test matrix is shown in Fig. 4.

This was extended in the current work to include an equivalent counter gravity casting. The intent was to extend process understanding and test the hypothesis that counter gravity casting could reduce or eliminate Nb segregation.

2.1 Casting Procedure

Figure 5 shows the three mold geometries considered; the thin and thick conventional molds, and thin counter gravity mold. All three mold geometries include a partially stabilized zirconia (PSZ) ceramic foam filter.

The molds were machined from a solid log of 2020 grade graphite [6]. 2020 is a fine-grain isotropic graphite commonly used for molds and crucibles for the casting of uranium. To prevent chemical reaction between the molten uranium and the graphite mold, those parts of the mold and crucible that come in contact with molten uranium were coated with a yittrium-oxide (yittria) mold coating [7]. The yittria mold coating contains approximately 1/2% cellulose based binder in an alcohol carrier. The mold coating was applied with an automotive style paint sprayer and allowed to dry prior to mold assembly.

The casting was instrumented with a total of twenty thermocouples and the time temperature history recorded with a computer based data acquisition system. Twelve stainless steel sheathed type-K thermocouples (chromel – alumel) were inserted into holes drilled in the graphite mold (1.6 mm or 1/16" OD). Eight alumina sheathed type-C thermocouples (W-5%Re – W-26%Re) with a bare-bead tip were routed through holes in the mold wall and into the casting cavity. The 3.2 mm (1/8") OD alumina sheathes were then cemented in place to prevent the thermocouples from being pushed out by the hydrostatic (metastatic) pressure of the molten metal. Locations of the thermocouples are shown in Fig. 5.

Figure 6 shows a photo of the conventional top fill casting mold assembly prior to the addition of the insulation layers and induction heating coils. Figure 7 shows the mold components of the 120 mm diameter counter gravity mold prior to assembly. The white coating is the yittria mold coating. Figure 8 shows the detail of the bottom of the down-sprue/filter holder with the ceramic foam filter in place. Figure 9 shows the counter gravity casting mold assembly prior to installation of the induction heating coils and insulation.

Again, the stainless steel sheathed type-K thermocouples are the silver wires while the alumina sheathed type-C thermocouples are the segmented white strands.

The crucible was charged with U-6wt%Nb cut from VIM-VAR-VAR ingots. Table 1 shows the charge weight, used for the individual the 120 mm cylinder castings.

The mold stacks were placed in LANL's K-furnace. This furnace is a three-zone vacuum induction melting (VIM) furnace. The three independently controlled induction coils heat the crucible, the mold top and the mold bottom. The crucible has a 35kW power supply operating at nominally 9.6 kHz and he mold coils are 50 kW at nominally 3 kHz. The location of the top and bottom mold coils are shown in Fig. 10. The furnace vacuum is produced by a rotary-vane mechanical vacuum pump.

2.2 Casting Results

In Fig. 11 the thermal history during heat up and casting of the thin conventional 120 mm cylinder mold cast at the nominal temperature is shown. The other two conventional top-poured castings had similar behaviors. In Fig. 12 the thermal history during heat up and casting of the counter gravity 120 mm cylinder mold casting is shown. Also shown in these plots is the induction power levels for the crucible, mold top, and mold bottom coils. In both cases crucible power was applied 15 or 20 minutes prior to mold heating to make sure that the metal was at the desired temperature at the same time that the mold was at the desired temperature for pouring. All 4 castings were poured at 1445°C (a superheat of 120°C above the liquidus temperature). Table 1 shows the charge weight, casting weight, and casting yield for these castings.

In Fig. 13 the temperature as a function of position (thermal gradient) for the conventional top fill and counter gravity 120 mm cylinder castings at pour time is shown. Origin of Z is the bottom of the casting. As was intended the thin and thick castings at the regular casting temperature had the same initial mold temperature. The hot casting had nearly the same thermal gradient and is approximately 200°C warmer. The counter gravity had a negative thermal gradient as intended, but this thermal gradient was less than was hoped for.

The appearance of the thin conventional 120 mm cylinder casting cast at the regular temperature, is shown in Fig. 14 in the as-cast state. The graphite core is still in the casting and the tips of the type-C thermocouples are imbedded in the metal. The appearance of the counter gravity 120 mm cylinder casting is shown in Fig. 15 in the as-cast state. The graphite core is still in the casting and the tips of the type-C thermocouples are imbedded in the metal.

In Figures 16 though 18, the thermal history of the thermocouples in the casting cavity are plotted as a function of time for the various 120 mm cylinders. The solidus (1255°C) and liquidus (1325°C) are also indicated by dotted lines. From these cooling curves the solidification time (time to reach solidus temperature) and the local solidification time (time between reaching liquidus and solidus temperatures) can be determined. Table 2 shows

the solidification time and local solidification time as a function of location for the 120 mm cylinder castings.

In Fig. 19 the Nb concentrating is plotted as a function of position in the casting. Chemical analysis was performed using ICP-MS on chip samples taken from drillings. In Fig. 20 the Nb concentration is replotted next to scale drawings of the cross section of the casting mold/wall for better perspective. The conventional top fill castings all have significant inverse Nb segregation. With the thick casting having the worse segregation and the thin casting with normal initial mold temperature being the best. The counter gravity casting has a far more uniform Nb concentration, with the composition being constant in the bulk of the cylinder and some slightly higher Nb values at the top.

2.3 Summary of Small Cylinder Results

For U-6wt%Nb castings solidified conventionally from bottom-to-top:

- Segregation is most strongly related to solidification time
- Macro-segregation is most severe in the bottom of the conventional castings; this is the region which also solidifies most rapidly
- For similar solidification times, there appears to be a thickness effect (for the 8 to 16 mm thickness examined)

For casting with counter gravity solidification (top-to-bottom):

- Macro-segregation is mostly eliminated
- A higher thermal gradient than obtained in this experiment would be beneficial to better cast structure and a better cast part

The observed macro-segregation is consistent with free-dendritic growth with flotation (buoyancy driven and/or filling driven advection of liquid).

3. Large 250 mm Diameter Cylinders

Based on the improved segregation behavior of the small counter gravity cast cylinder, the same approach was applied to a larger casting to scale-up the process. The casting geometry chosen is nominally 250 mm in diameter with a 12.5 mm thick wall and is 310 mm tall.

3.1 Initial Mold Design

3.2.1 Mold Design

The counter gravity mold design used for the 120 mm cylinder was scaled up to 250 mm diameter. This mold design is shown in Fig. 21. The LANL three-zone vacuum induction furnace only can accommodate a mold that is less than 635 mm tall. Because of this limitation, the length of the casting is restricted. The position of the 250 mm counter gravity mold as it is positioned in the furnace is shown in in Fig. 22. Also shown are the heating coils and crucible with stopper rod.

An additional change in this scaled up mold design was to move the feeder (hot top) at the bottom of the casting from the outer diameter of the part (as it is on the 120 mm mold) to the inner diameter of the part. This change allows the outer diameter to be reduced and allows the mold to fit in the 350 mm ID mold heating coils.

For this design, the goals for mold temperature at pour time are

- Funnel hot, mold top cool, base hot
- Need high negative thermal gradient between mold top and base to drive solidification down with enough gradient to avoid porosity
- Need hot base with filter temperature greater than the liquidus temperature.

Need to keep down-sprue hot to allow it to act as feeder during solidification

- To maintain pressure and avoid macro-porosity the down sprue needs to solidify after part – the sprue is the feeder (hot top)
- Sprue needs to have enough molten liquid to feed part shrinkage during solidification

Further, the funnel acts as susceptor to heat down-sprue. At the same time, inductive coupling between the funnel coil and mold top has to be avoided. If there is too much coupling the mold top will be heated and the desired thermal gradient will not be obtained. To avoid coupling, the distance between the funnel and the mold top should be maximized. But because we are severely limited by furnace height this was where a design compromise had to be made. As will be seen, this is where the design failed.

3.2.2 Process Simulation of Initial Mold Design

In order determine a best set of casting parameters, a set of processing simulations where conducted. Mold filling and solidification was simulated using the commercial computational fluid dynamics code Flow-3D [8]. FLOW-3D solves relevant time-

dependent heat and fluid flow free-surface problems in three dimensions. Flow-3D can't include induction heating, so the simulations must assume an initial mold temperature and the simulation begins with mold filling.

Figure 23 shows the simulation setup including the mold geometry, initial temperature distribution, and mesh/simulation boundaries. The simulation was performed in 3D with quarter symmetry. Four different conditions are considered. Table 3 shows the initial and boundary conditions used for simulation of filling and solidification of revision C counter gravity 250 mm cylinder. The initial conditions are shown graphically in Fig. 24.

Various thermophysical and other boundary conditions used are discussed in greater detail in Appendix A.

Figures 25 and 26 show the fraction solid as a function of time for the four simulations. Qualitatively the four different sets of conditions are similar. Based on the fact that the sprue stays molten slightly longer for the A4 simulation conditions, the goal for the casting will be a pour temperature of 1460°C (135°C superheat) and mold base of 1155°C.

3.2.3 Casting of Initial Mold Design

The counter gravity 250 mm cylinder casting with mold revision A has LANL casting number 17K-695. Figure 27 shows the mold components after mold coating and prior to assembly. The layout of thermocouples, induction coils, and insulation for the casting is shown in Fig. 28. Table 5 shows the charge weight, casting weight, and casting yield for the 250 mm cylinder castings.

The thermal history during heat up and casting is shown in Fig. 29. Unfortunately, the top mold coil coupled with the top of the mold and the mold top became much warmer than the goal temperature. This is illustrated better in Fig. 30, where the temperature as a function of position from the bottom of the casting at pour time is plotted. Black lines are actual temperature; purple lines are desired temperature.

At pour time, the stopper rod was pulled and induction power was cut. Unfortunately, the stopper rod mechanism malfunctioned and the stopper rod was not withdrawn. No metal poured into the mold and metal remained in the crucible where it solidified.

Although this was a failed casting because of the stopper rod failure, it is believed (based on the lack of a thermal gradient in the mold) that if the casting had poured that a bad casting would have resulted. Based on the undesirable inductive coupling between the top mold coil around the funnel and mold top it was decided that the casting would not be recast with this mold/coil configuration. This coupling problem is a fundamental problem with the mold design and not something that different heating or induction power profiles would solve.

3.3 Revised Mold Design

3.3.1 Mold Design

In order to eliminate the undesirable inductive coupling between the top mold coil (around the funnel) and mold top, observed in the initial configuration, it was decided that a small unheated funnel would be used with the same mold for the next casting. It was hoped that there would be sufficient heat transfer from the base to preheat the down-sprue. To provide a heat sink at the top of the mold a 50 mm thick steel “chill” was placed on top of the mold. This configuration is referred to as mold revision B.

A third configuration was investigated. In this version (revision C), all of the components are the same as revision B, but the case has been modified by thinning it to give a 14.5 mm thick casting.

In Fig. 31 the three versions of the 250 mm diameter cylinder counter gravity mold is compared along with the coil positions used.

3.3.2 Process Simulation of Revised Mold Design

In order determine a best set of casting parameters, Flow-3D was again used to simulate as set of processing conditions. The mesh and simulation conditions are identical to those shown in Fig. 23, but with a different mold geometry. Table 4 lists the initial and boundary conditions used for these simulations with the revision C mold. The initial mold temperature distributions are also show graphically in Fig. 32.

Simulation results of the three different sets of mold and pouring temperatures are shown as a function of time in Fig. 33 through 37. Again, the three different sets of conditions are similar qualitatively. Based on this lack of qualitative difference, it was decided to use the C2 conditions for the casting. The goal is to poured at a temperature of 1460°C (135°C superheat) and a mold base temperature of 1155°C. This is the same set of goal temperatures that had been intended to be used for the initial casting.

3.3.3 Casting of Revised Mold Design

Second Casting 17K-696

The layout of thermocouples, induction coils, and insulation for casting 17K-696 with counter gravity 250 mm cylinder mold revision B are shown in Fig. 38. The mold, core, base, and sprue are identical to the initial casting. The large funnel has been replaced with a small funnel and a steel chill has been placed on the top of the mold. The mold assembly prior to installation of the induction heating coils and insulation is shown in Fig. 39. The stainless steel sheathed type-K thermocouples are the silver wires. Blue painters tape on the funnel top keeps mold interior clean during assembly and is removed prior to casting.

Figure 40 shows the thermal history during heat up and casting of the revision B counter gravity 250 mm cylinder casting 17K-696. The resulting casting is shown in Fig. 41. The casting did not fill the entire mold cavity leaving a 30 mm gap on the one side. Also evident

are patches of surface connected spongy porosity in the bottom 80 to 100 mm of the casting. In in Fig. 41 these patches are the dark areas near the bottom of the casting. The thermocouple profiles indicate that the sprue was not able to remain molten during the solidification of the bottom of the casting. As indicated before, if the sprue does not remain molten to keep the casting pressurized porosity will form in the casting.

Third Casting 17K-698

The layout of thermocouples, induction coils, and insulation for casting 17K-698 with counter gravity 250 mm cylinder mold revision c are shown in Fig. 42. The mold, core, base, and sprue are identical to the initial casting. The large funnel has been replaced with a small funnel and a steel chill has been placed on the top of the mold. Fig. 42

Figure 43 shows the thermal history during heat up and casting of the revision C counter gravity 250 mm cylinder casting 17K-698. The resulting casting is shown in Fig. 44. Again, patches of surface connected spongy porosity in the bottom 100 of the casting are evident. The thermocouple profiles indicate that the sprue was not able to remain molten during the solidification of the bottom of the casting.

3.4 Discussion and Summary of Initial Large Cylinder Results

Figure 45 shows the thermal gradient at pour time for the three counter gravity 250 mm cylinder castings. As mentioned in section 3.2.3, the first casting (17K-695) with the heated funnel did not have the large negative thermal gradient in the mold that is needed to successfully produce a sound counter gravity casting. The second two castings (17K-696 and -698) had a good negative thermal gradient in the mold body. Unfortunately for these two, there was not the strong positive thermal gradient in the sprue and funnel. As such these two castings were unable to maintain metal pressure during solidification and porosity resulted.

For a good casting, what is needed is the best of both; a strong positive thermal gradient in the sprue and funnel along with a strong negative gradient in the mold body.

4. Path Forward for Large Cylindrical Castings

On the left side of Fig. 46 the furnace with counter gravity mold stack is shown with the desired initial temperatures. The height limitations of the current LANL three-zone furnace does not allow the needed separation of the funnel from the mold top (for a reasonably tall cylinder). Upon careful consideration, it becomes apparent that there is an inherent redundancy in this design, in that there is the very hot crucible above the hot funnel.

If the down-sprue was extended all the way to the crucible, and the crucible sealed against the down-sprue, the funnel would be unnecessary. Such funnel-less approach is shown on right side of Fig. 46. Such a mold design would have the same goals discussed in Section 3.2.1, but now the crucible would be used to heat the down-sprue and maintain mold pressurization during solidification.

Such a funnel-less approach has several major advantages:

- Creates significant separation between crucible coil and top of mold to avoid coupling between top coil and the top of the mold thereby keeping the top of the mold cool.
- Increases furnace height limits; allowing for a taller casting.
- Allows the crucible to be used as feeder thereby reducing metal usage.
- Allows longer down sprue for additional pressurization of the casting.

This approach has not yet been proven experimentally. In FY'18 follow on work will to try to implement this approach. Work needed includes:

- Modifications to the furnace crucible support.
- Truchas induction heating modeling to determine needed separation between mold top and crucible to avoid coupling – how tall can the casting be?
- Flow and solidification modeling to appropriately size sprue and other mold components.
- Actual casting trials.

5. References

[1] B.A. Rogers, et al, Trans. Metall. Soc. AIME (1958)

[2] D. J. Thoma, unpublished data (2004)

[3] W.D. Drotning, High Temp. High Press., 14, 253-258 (1982)

[4] Smithells Metals Reference Book, Ed. W.F. Gale and T.C. Totemeier, Elsevier Butterworth Heinemann, Boston, Eighth Ed. 2004.

[5] W. Kurz and D.J. Fisher, Fundamentals of Solidification, Trans Tech Pub (1984).

[6] 2020 grade graphite by Mersen, St. Marys, PA.

[7] Type YK nonaqueous-based yttrium oxide paint by ZYP Coatings, Oak Ridge, TN USA.

[8] Flow-3D by Flow Science Inc., Santa Fe, NM USA.

[9] Thermophysical Properties of High Temperature Solid Materials, Vol. 1: Elements, The MacMillian Co. (1967)

[10] I. Barin, “Thermochemical Data of Pure Substances”, 3rd Ed., VCH (1995).

[11] Graphite Design Handbook, DOE-HTGR-88111 (1988).

Tables

Table 1
Charge weight, casting weight, and casting yield for the 120 mm cylinder castings.

Casting Description	Charge wt (kg)	Casting wt (kg)	Casting Yield
Thick (16 mm) / Regular Mold Temperature	28.07	25.28	0.90
Thin (8 mm) / Hot Mold Temperature	15.02	13.47	0.90
Thin (8 mm) / Regular Mold Temperature	15.13	13.36	0.88
Counter Gravity Thin (8 mm)	28.01	20.26	0.72

Table 2
Solidification time and local solidification time as a function of location for the 120 mm cylinder castings.

		Cavity							Down Sprue
	Thermocouple ID	TC20	TC19	TC18	TC17	TC16	TC15	TC14	TC13
	Distance from Bottom, Z (mm)	5	20	40	85	130	175	205	
Solidification Time (s)	Thin/Hot	5	7	11	109	217	298	506	
	Thin/Regular	3	4	6	14	54	107	206	
	Thick/Regular	4	6	8	59	198	312	389	
	Distance from Top (mm)	5	20	40	85	130	175	205	-25
	Distance from Bottom, Z (mm)	240	225	205	160	115	70	40	270
Solidification Time (s)	Thin / Top Down	17	74	158	176	275	239	244	365

	Distance from Bottom, Z (mm)	5	20	40	85	130	175	205	
Local Solidification Time (s)	Thin/Hot			7	100	206	211	252	
	Thin/Regular			3	9	49	103	165	
	Thick/Regular				53	174	264	326	
	Distance from Top (mm)	5	20	40	85	130	175	205	-25
	Distance from Bottom, Z (mm)	240	225	205	160	115	70	40	270
Local Solidification Time (s)	Thin / Top Down	8	69	158	168	269	233	239	636

Table 3

Initial and boundary conditions used for simulation of filling and solidification of revision A counter gravity 250 mm cylinder.

	Initial Mold Base Temperature		Initial Mold Top Temperature		dT/dZ Case	Pour Temperature	
Simulation		°C		°C			°C
CG_250_Cylcinder_Sim-A1	Tsolidus	1255	Tsolidus-355	900	-1000	85° superheat	1410
CG_250_Cylcinder_Sim-A2	Tsolidus-50	1205	Tsolidus-355	900	-859	85° superheat	1410
CG_250_Cylcinder_Sim-A3	Tsolidus-100	1155	Tsolidus-355	900	-718	85° superheat	1410
CG_250_Cylcinder_Sim-A4	Tsolidus-100	1155	Tsolidus-355	900	-718	135° superheat	1460

Table 4

Initial and boundary conditions used for simulation of filling and solidification of revision C counter gravity 250 mm cylinder.

	Initial Mold Base Temperature		Initial Mold Top Temperature		dT/dZ Case	Pour Temperature	
Simulation		°C		°C			°C
CG_250_Cylcinder_Sim-C1	Tsolidus-100	1155	Tsolidus-355	1173	-718	135° superheat	1460
CG_250_Cylcinder_Sim-C2	Tsolidus-100	1155	Tsolidus-505	1023	-1141	135° superheat	1460
CG_250_Cylcinder_Sim-C3	Tsolidus-100	1155	Tsolidus-505	1023	-1141	85° superheat	1410

Table 5
Charge weight, casting weight, and casting yield for the 250 mm cylinder castings.

Casting Description	Casting ID	Mold Revision	Charge wt (kg)	Casting wt (kg)	Casting Yield
Counter Gravity 12.5 mm Thick with Heated Funnel	17K-695	A	83.98	0	-
Counter Gravity 12.5 mm Thick with Cold Funnel	17K-696	B	83.41	78.50	0.941
Counter Gravity 14.5 mm Thick with Cold Funnel	17K-698	C	100.30	96.50	0.962

.

Appendix A

Boundary Conditions and Thermophysical Properties Used for Filling Simulations.

MESHING
Use 3 mesh blocks
Break mold body into upper and lower objects to minimize simulation size
Grid size = 2.0 mm in most areas; 1.67 mm in mold cavities

INITIAL CONDITIONS:
Simulation dependent; see Table 3 and 5 and Figures 24, 25, and 32

BOUNDARY CONDITIONS
Metal pour temperature simulation dependent; see Table 3 and 5
Temperature at top of mesh = pour temperature, mesh simulation dependent
Temperature at bottom of mesh simulation dependent; see Figures 1, 23, and 32
No radiation from mold surface

Interfacial Heat Transfer Coefficients:
Fluid/Mold IHTC = 2000 W/m^2•K above liquidus
Fluid/Mold IHTC linear from 2000 to 500 between liquidus and solidus
Fluid/Mold IHTC = 500 W/m^2•K below solidus
Crucible/Mold IHTC = 200 W/m^2•K
Mold/Mold IHTC = 100 W/m^2•K

Thermophysical - Fluid

Used pure U viscosity and surface temperature properties from Smithals [4] since U-Nb data is unavailable
viscosity of liquid = 0.0065 kg/m•s (see best guess values for mushy zone effects)
surface tension coefficient = 1.55 N/m
surface tension coefficient temp sensitivity = -0.14E-3

Thermal conductivity of pure U from TPRC [9]

Temperature (K)	Therm. Cond. (W/m•K)
300	23.85
1100	42.26
1463	50.61
1504	25.3
2000	25.3

Enthalpies of U-Mo estimated from pure U data from Barin [10]
latent heat of transformation = 4.616E4 J/kg
specific heat of liquid = 201.3 J/kg•K
specific heat of solid = 181.1 J/kg•K

Solidus and liquidus based on linearized phase diagram informed by ref [1-2]
liquidus temperature =1598 K
solidus temperature =1528 K
reference temperature = 1408 K (tstar in Flow-3D)
reference composition =0.10 (cstar in Flow-3D)
partition coefficient = C_L/C_S = 1.727

Best guess values
static contact angle for fluid wall adhesion = 90 deg
dendrite coherency point = 0.16
critical fraction solid above with there is no fluid flow = 0.66
viscosity of liquid at dendrite coherency point = 0.0095 kg/m•s

Thermophysical - Graphite Mold

For specific heat times density and thermal conductivity use properties of grade 2020 from Graphite Design Handbook (1988) [11].

T (K)	Specific heat x Density ($J/K•kg^2$)	Thermal Conductivity (W/m•K)
250	1.0201E+06	
300	1.2687E+06	78.32
400	1.7628E+06	70.03
500	2.1674E+06	63.07
600	2.474E+06	57.33
700	2.7053E+06	52.66
800	2.8826E+06	48.97
900	3.0211E+06	46.13
1000	3.1314E+06	44.01
1100	3.2208E+06	42.50
1200	3.2943E+06	41.48
1300	3.3556E+06	40.83
1400	3.4073E+06	40.43
1500	3.4514E+06	40.15
1600	3.4893E+06	39.89
1700	3.5222E+06	39.51
1800	3.5509E+06	38.90
1900	3.5761E+06	37.94
2000	3.5984E+06	36.51

Figures

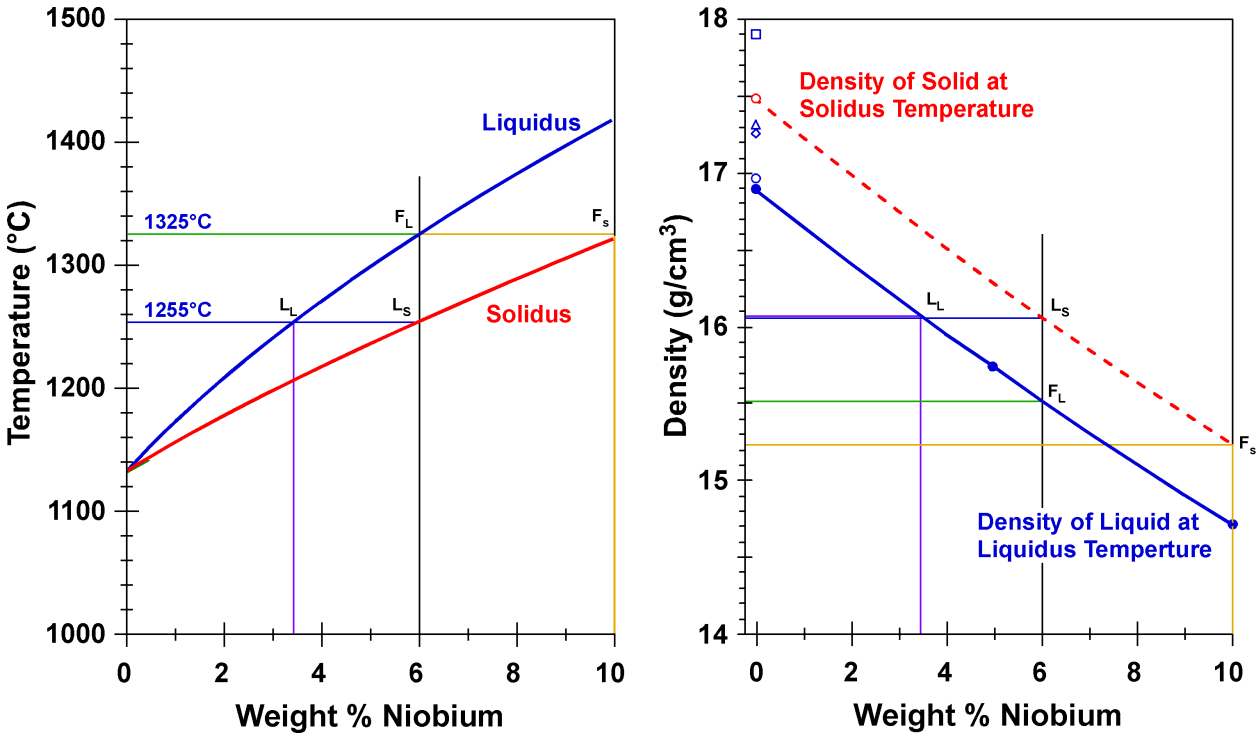

Fig. 1 Uranium rich side of uranium-niobium phase diagram (left) and density for solid and liquid at the melting point versus niobium content (right).

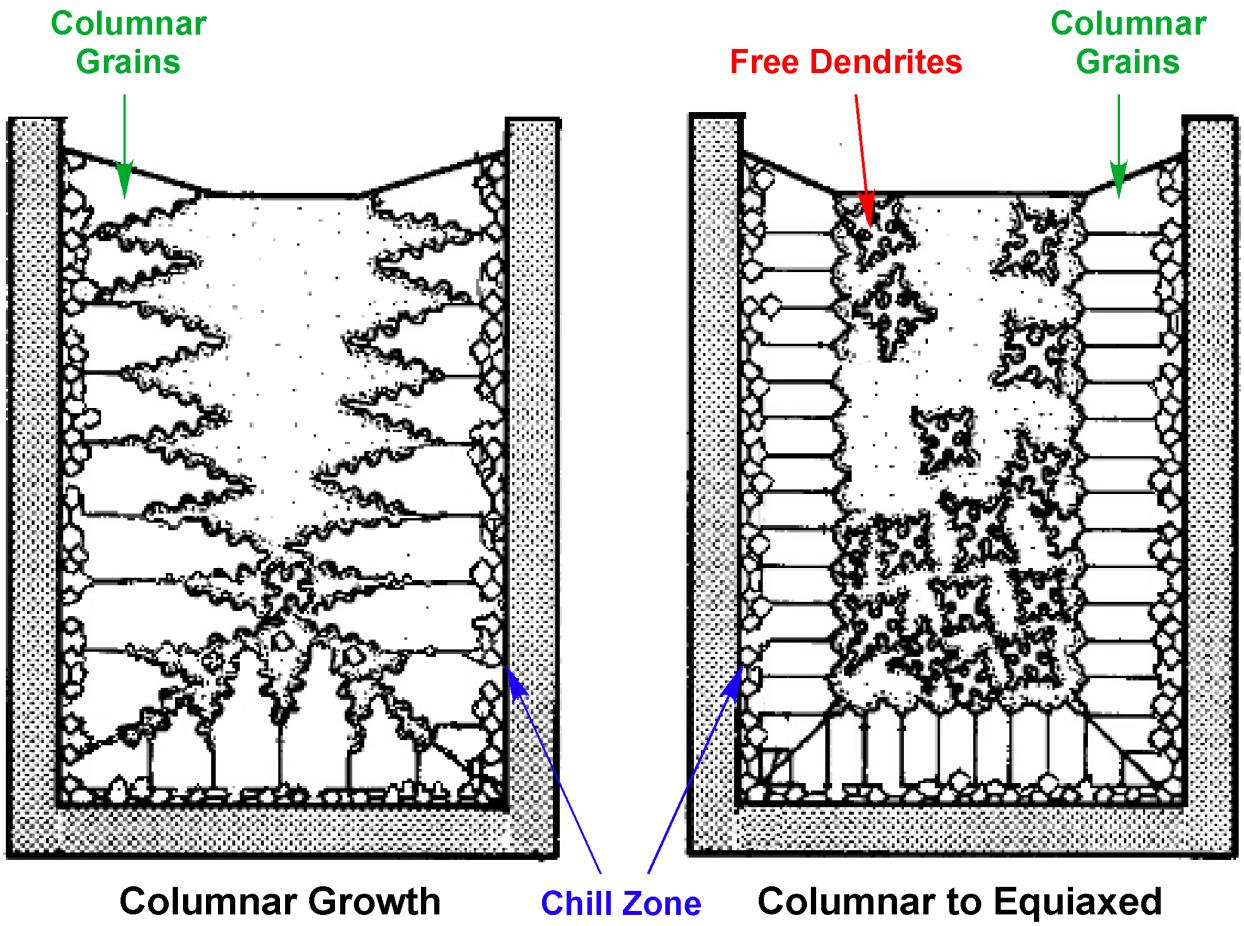

Fig. 2 Comparison of idealized solidification morphologies. In ingot on left solidification is by columnar grown. In ingot on right solidification started by columnar growth and transitioned to equiaxed free dendritic growth.

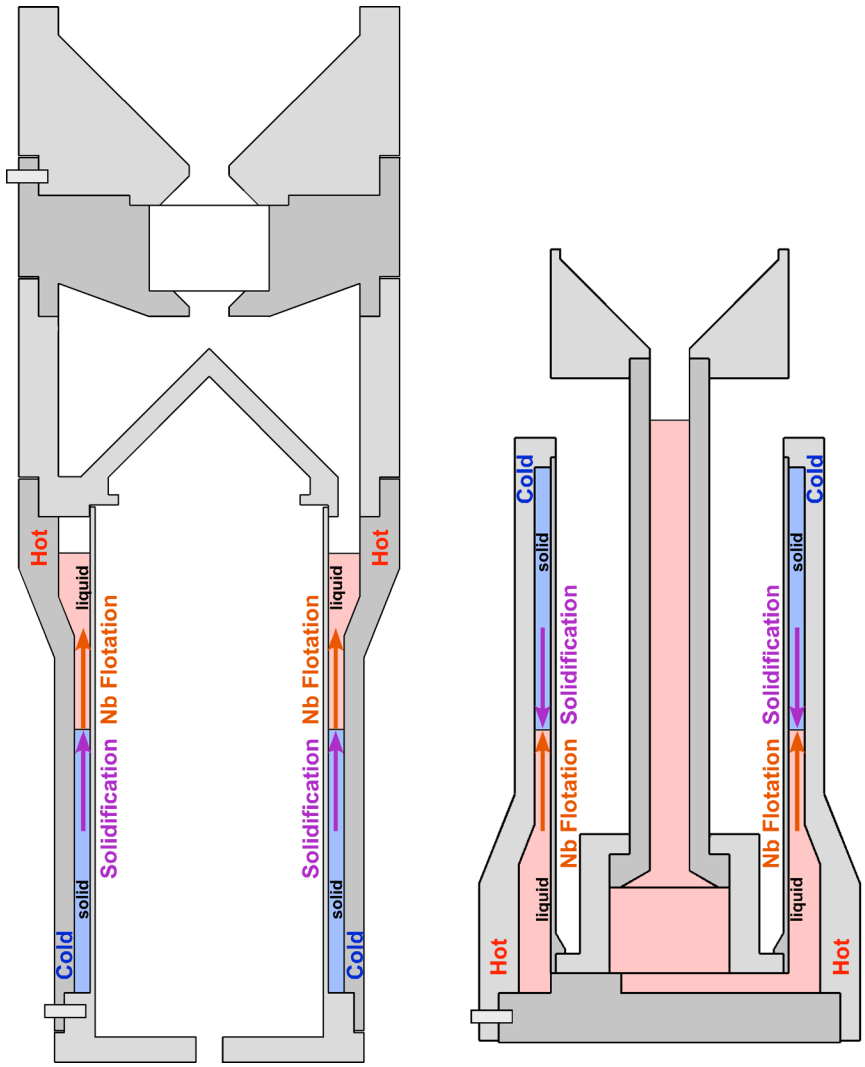

Fig. 3 Comparison of conventional top fill (solidify from bottom to top of mold) casting to counter gravity (bottom fill, solidify from top to bottom) casting.

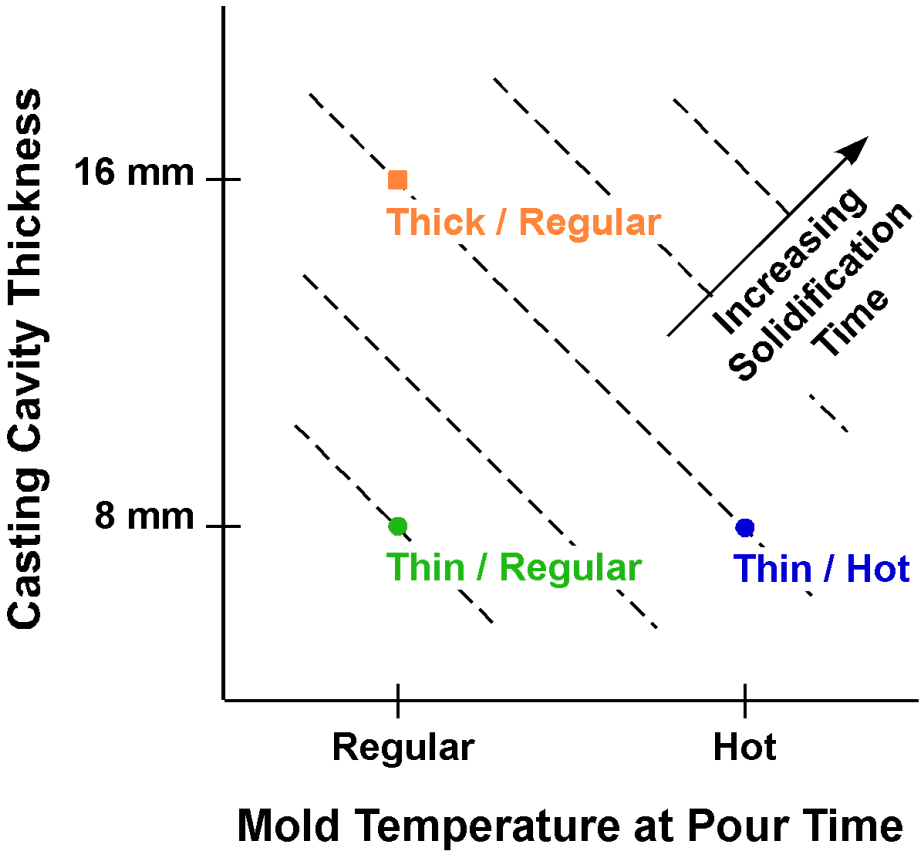

Fig. 4 Test matrix for the conventional top fill 120 mm castings.

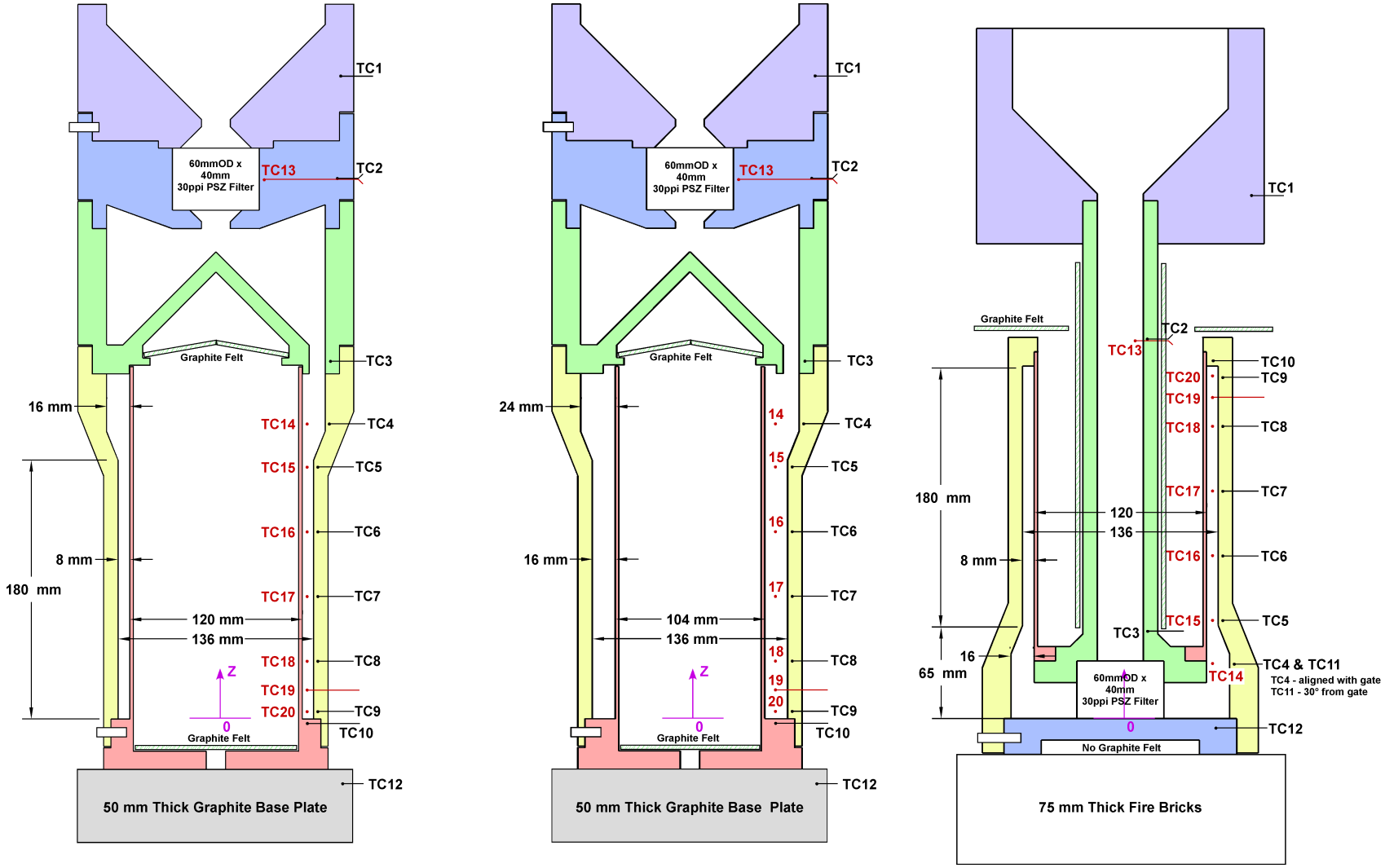

Fig. 5 Comparison of the thin and thick conventional molds, and thin counter gravity mold. The dimensions are given in mm. Locations of type-K thermocouples in the mold are indicated in black. Locations of type-C thermocouples in the casting cavity are indicated in red.

.

Fig. 6 Top fill casting mold assembly prior to installation of the induction heating coils and insulation. The stainless steel sheathed type-K thermocouples are the silver wires while the alumina sheathed type-C thermocouples are the segmented white strands. Blue painters tape keeps mold interior clean during assembly and is removed prior to casting.

Fig. 7 Mold components of the 120 mm diameter counter gravity mold prior to assembly. The white coating is the yittria mold coating.

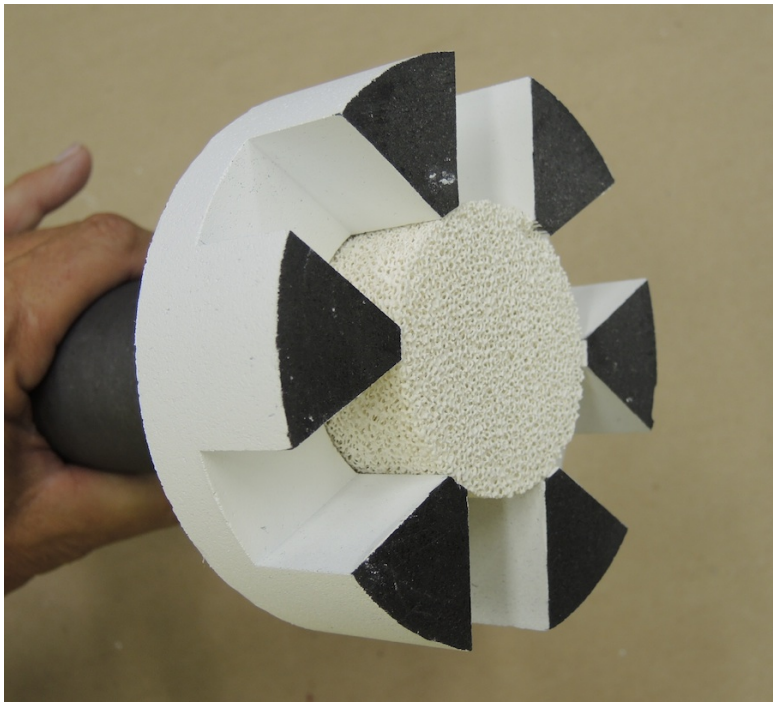

Fig. 8 Detail of the down-sprue/filter holder with porous ceramic filter in place.

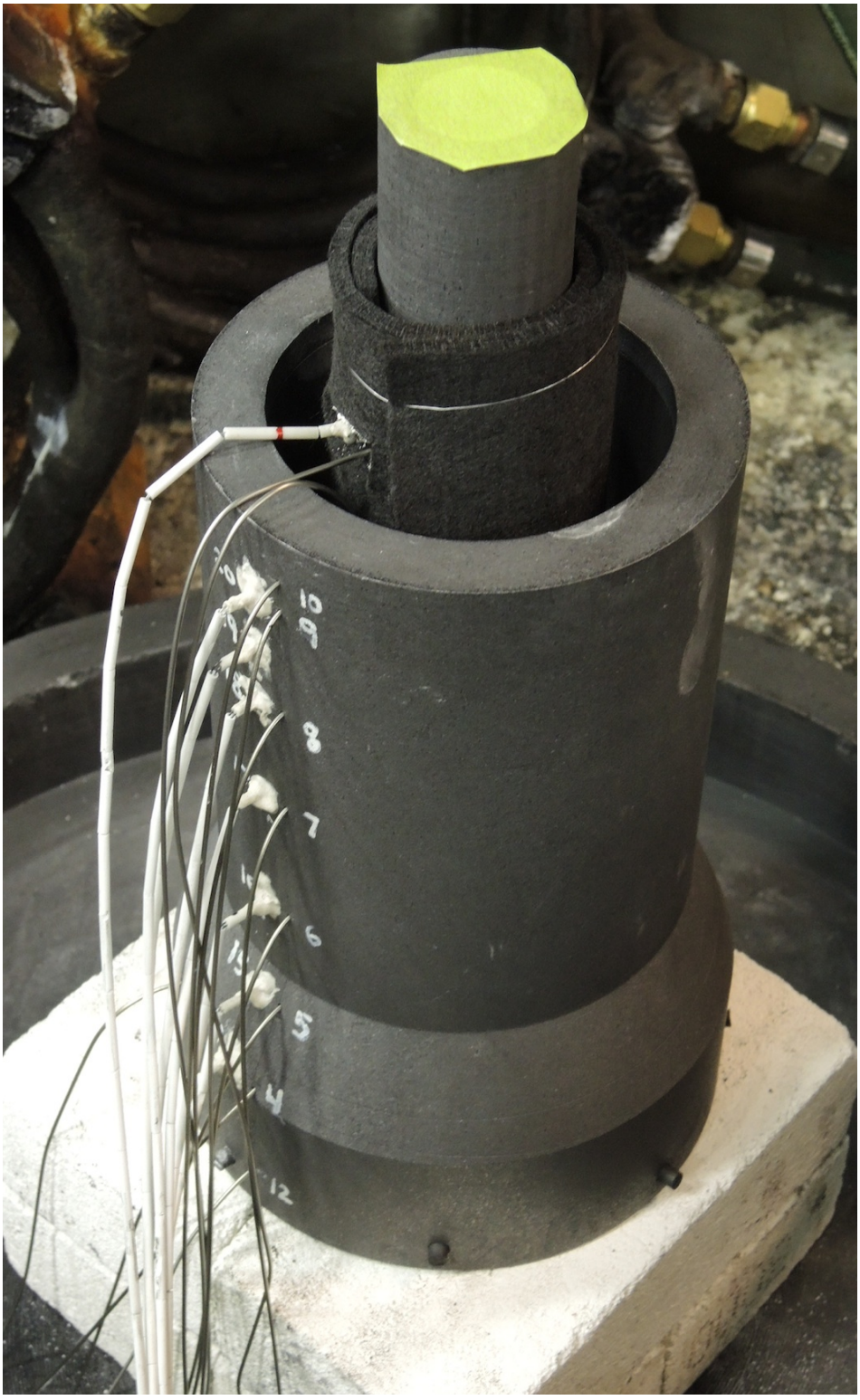

Fig. 9 Counter gravity casting mold assembly prior to installation of the induction heating coils and insulation. The stainless steel sheathed type-K thermocouples are the silver wires while the alumina sheathed type-C thermocouples are the segmented white strands. Green painters tape keeps mold interior clean during assembly and is removed prior to casting.

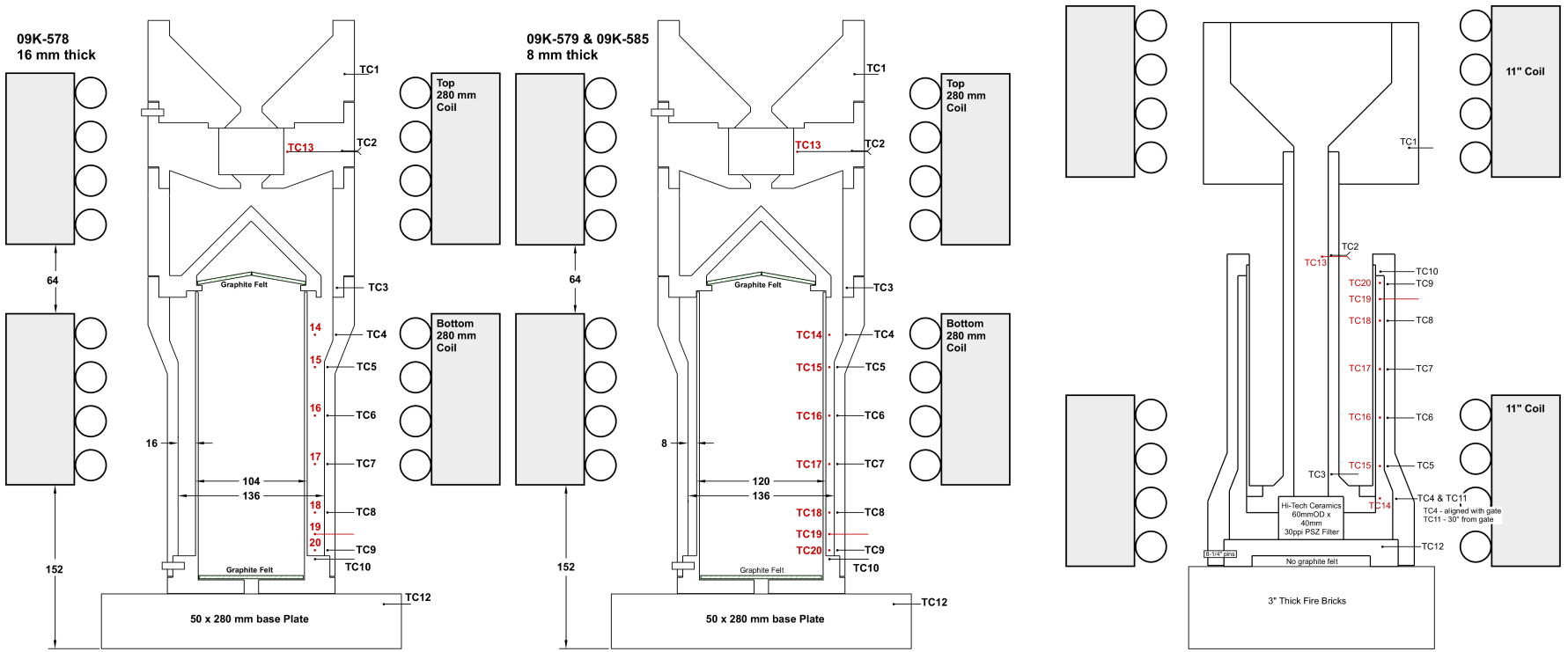

Fig. 10 Comparison of the three 120 mm cylinder molds of interest with the location of the induction heating coils indicated.

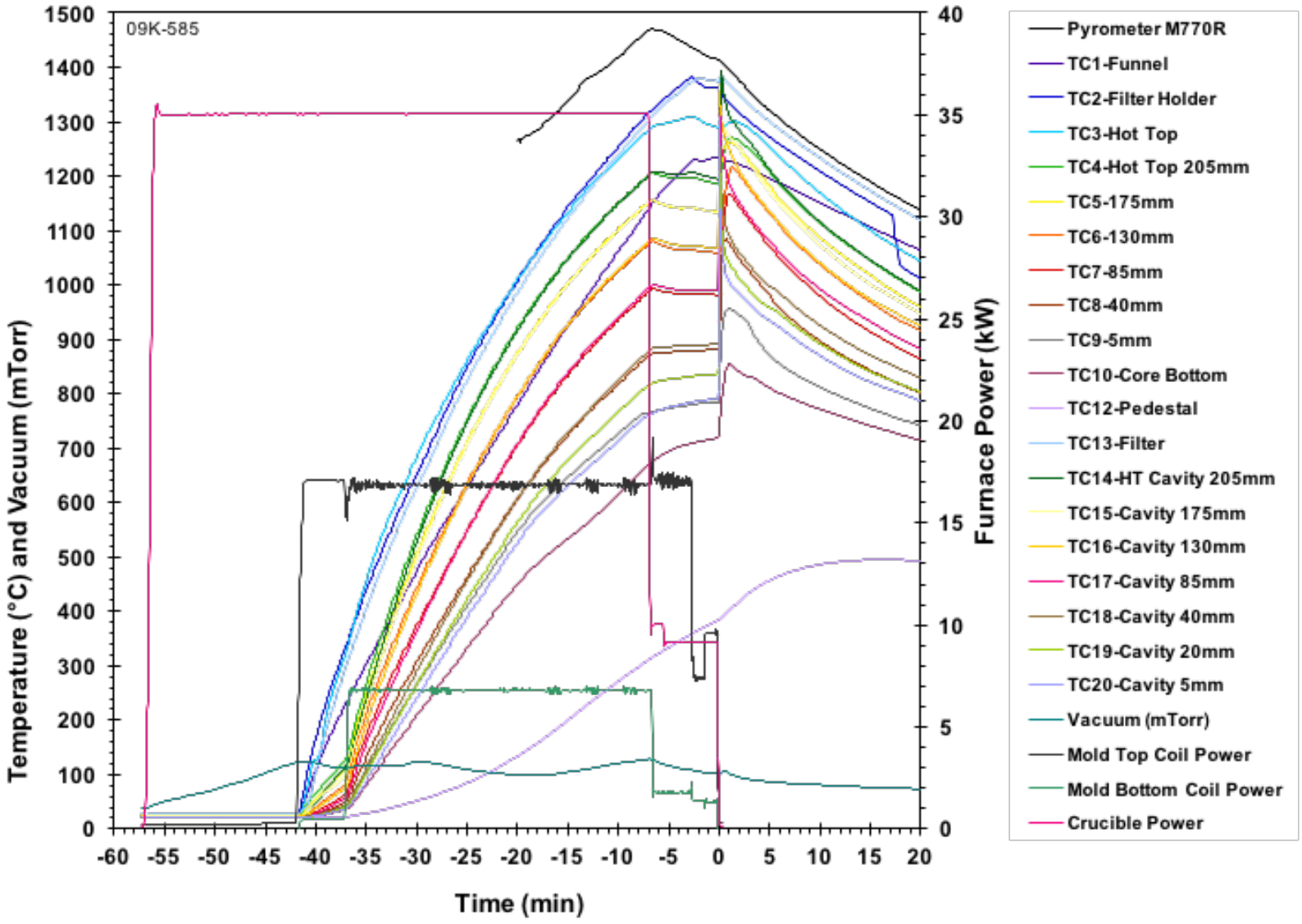

Fig. 11 Thermal history during heat up and casting of the thin conventional 120 mm cylinder mold cast at the nominal temperature.

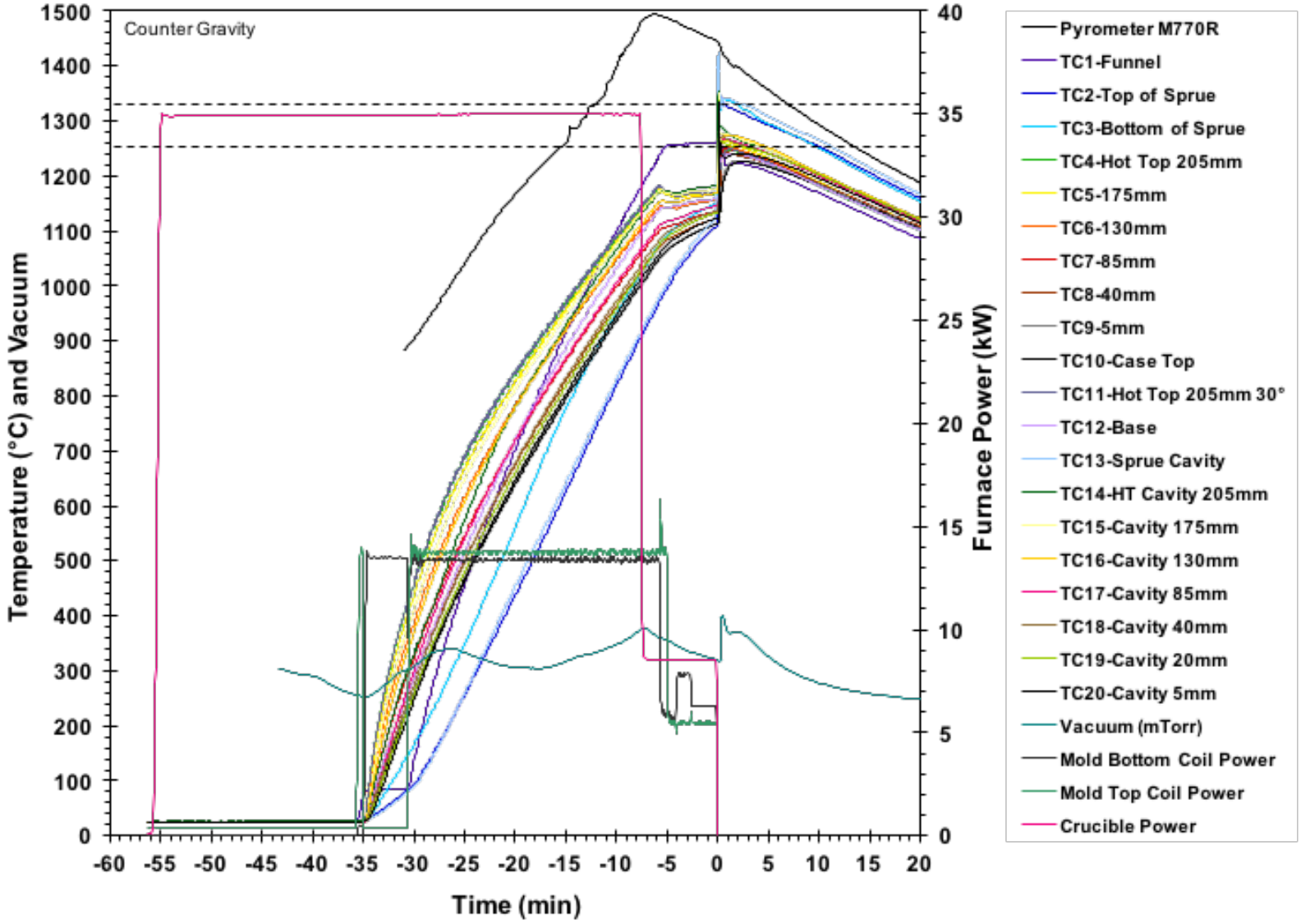

Fig. 12 Thermal history during heat up and casting of the counter gravity 120 mm cylinder mold casting.

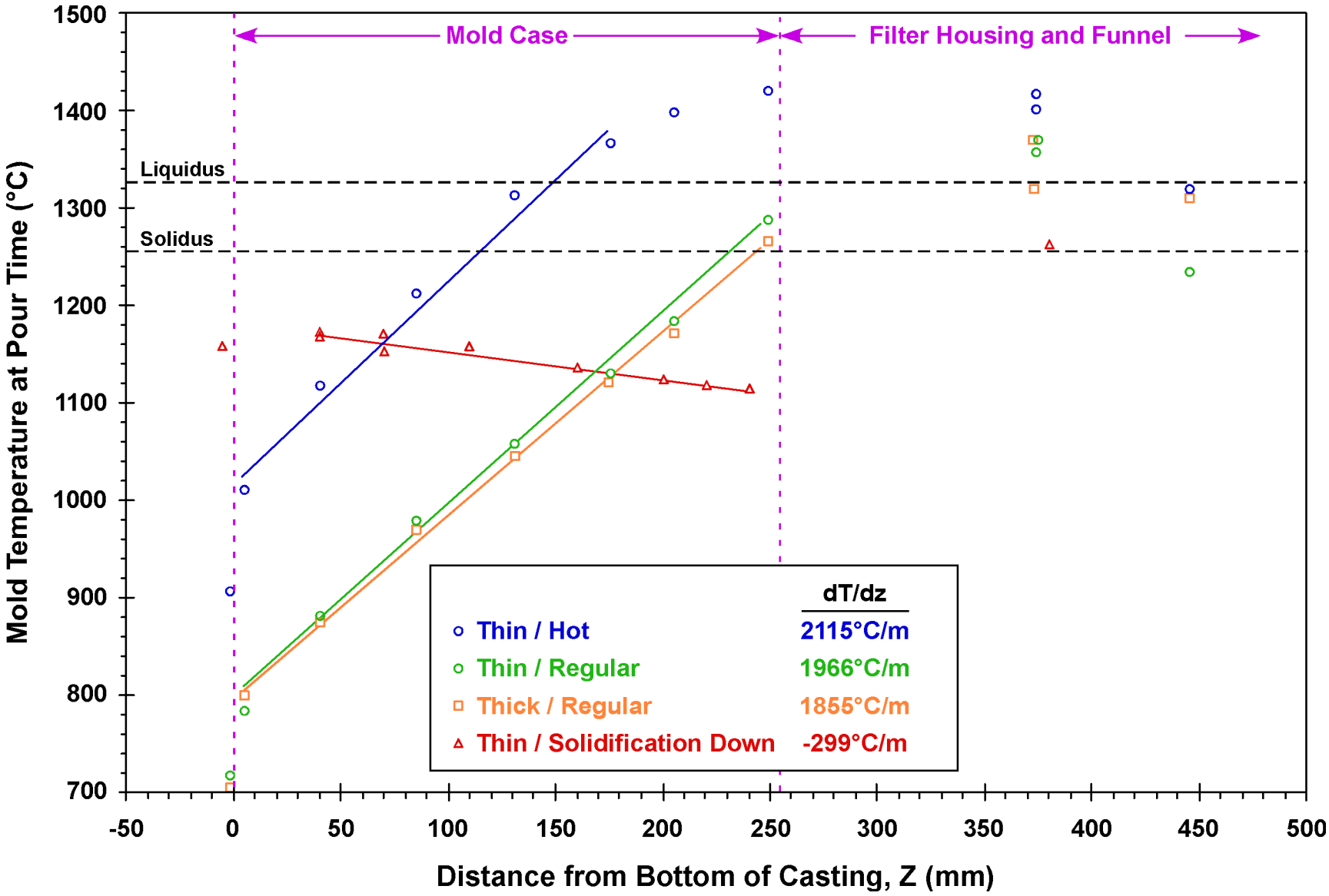

Fig. 13 Temperature as a function of position (thermal gradient) for the conventional top fill and counter gravity 120 mm cylinder castings at pour time. Origin of z is the bottom of the casting.

Fig. 14 Photograph of the thin conventional 120 mm cylinder casting, cast at the regular temperature, in the as-cast state. The graphite core is still in the casting and tips of the type-C thermocouples are imbedded in the metal.

Fig. 15 Photograph of the counter gravity 120 mm cylinder casting in the as-cast state. The graphite core is still in the casting and tips of the type-C thermocouples are imbedded in the metal.

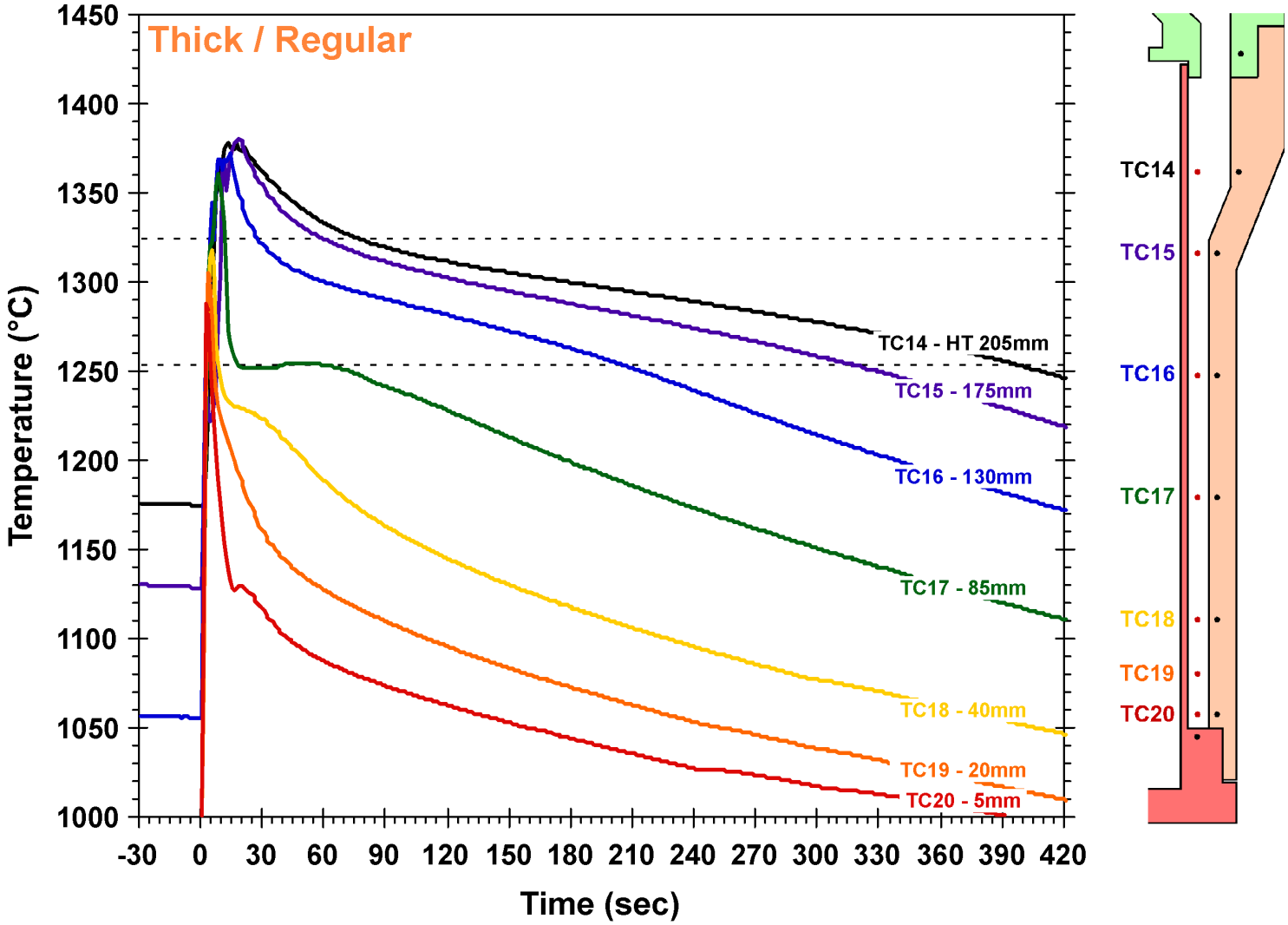

Fig. 16 Thermal history of the thermocouples in the casting cavity during pouring and casting of the thin conventional 120 mm cylinder mold cast at the nominal mold temperature.

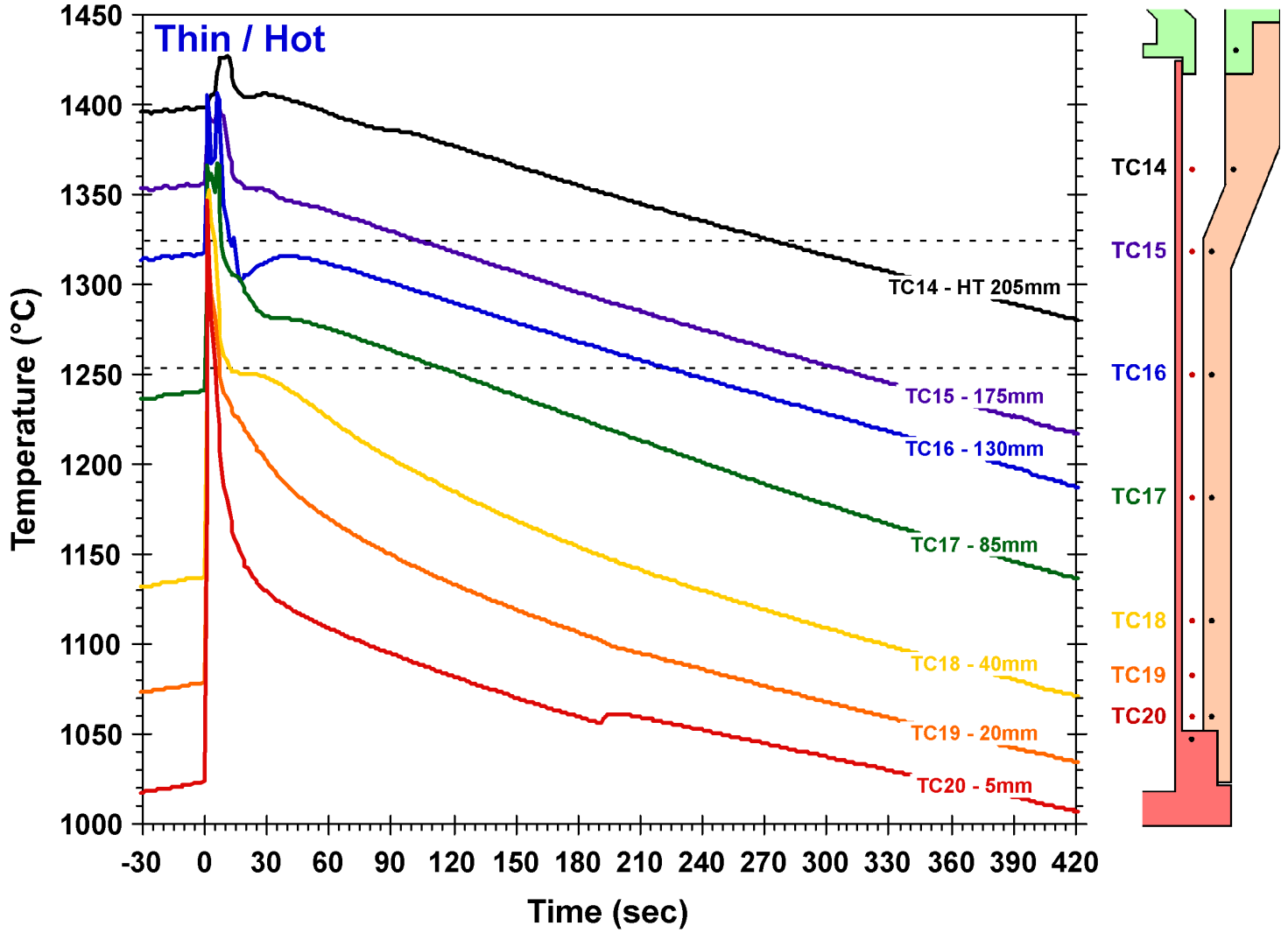

Fig. 17 Thermal history of the thermocouples in the casting cavity during pouring and casting of the thin conventional 120 mm cylinder mold cast at the hot initial mold temperature.

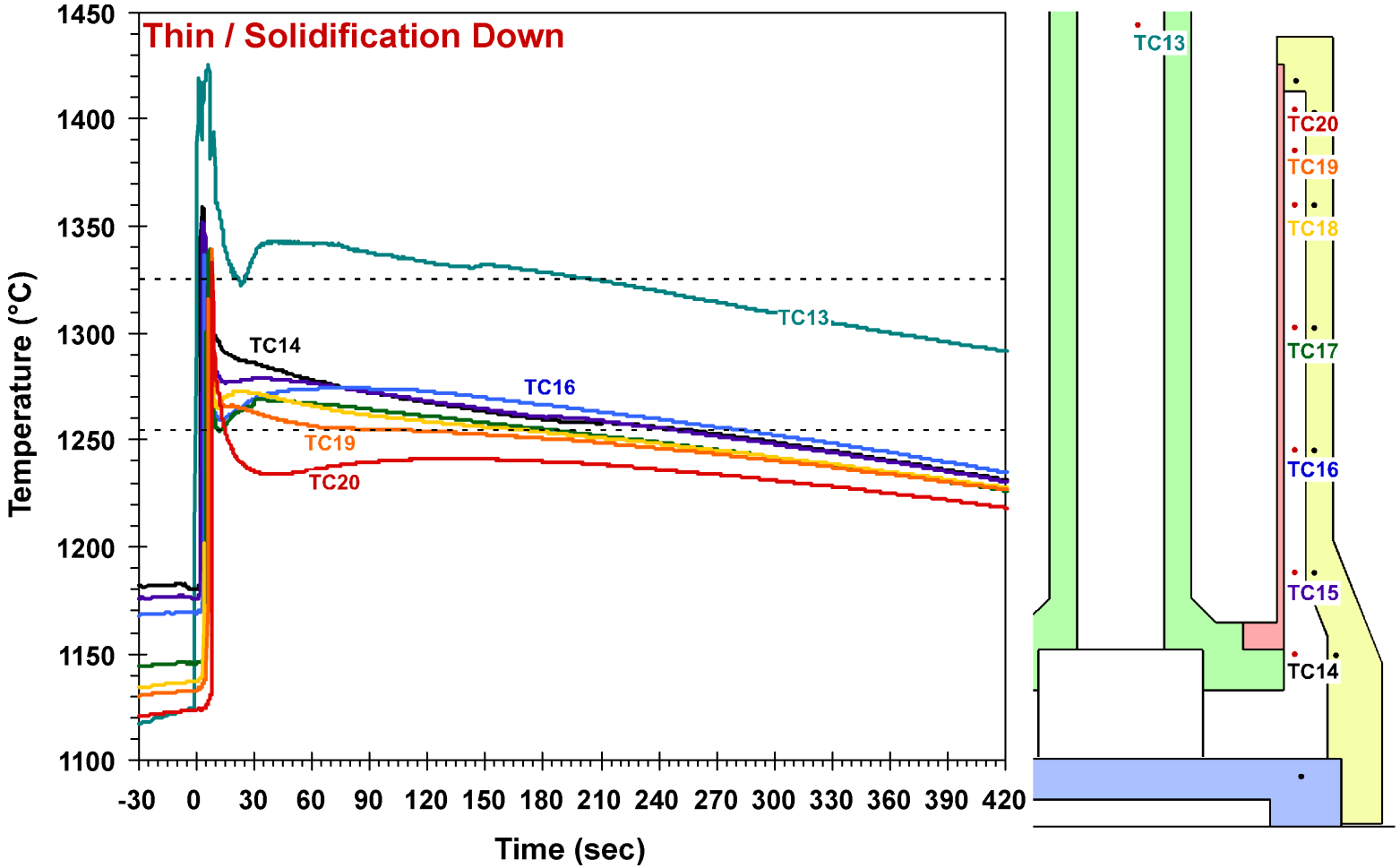

Fig. 18 Thermal history of the thermocouples in the casting cavity during pouring and casting of the counter gravity 120 mm cylinder mold.

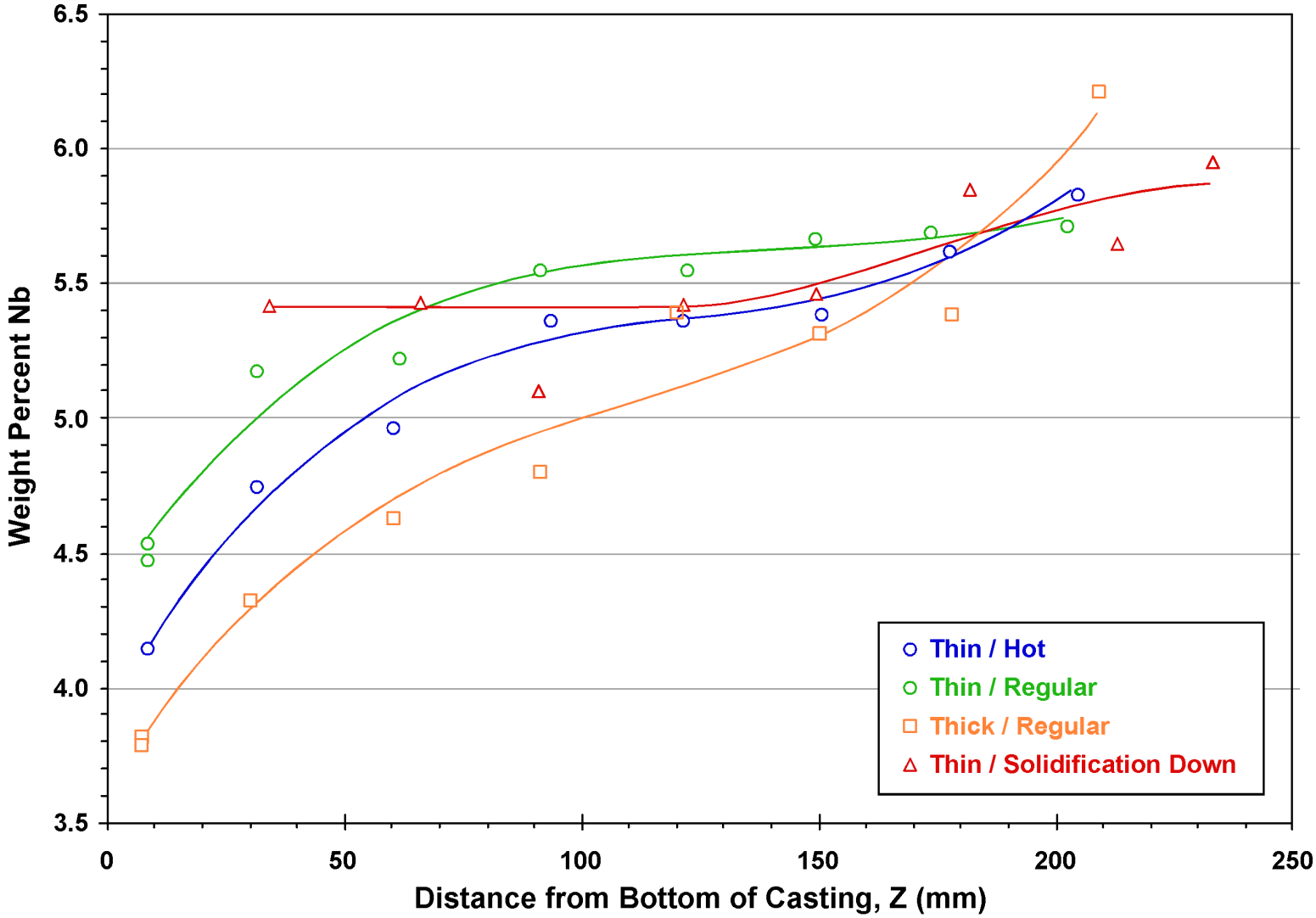

Fig. 19 Chemical analysis results as function of position. Samples from chips taken from 9 mm drill hole to casting center.

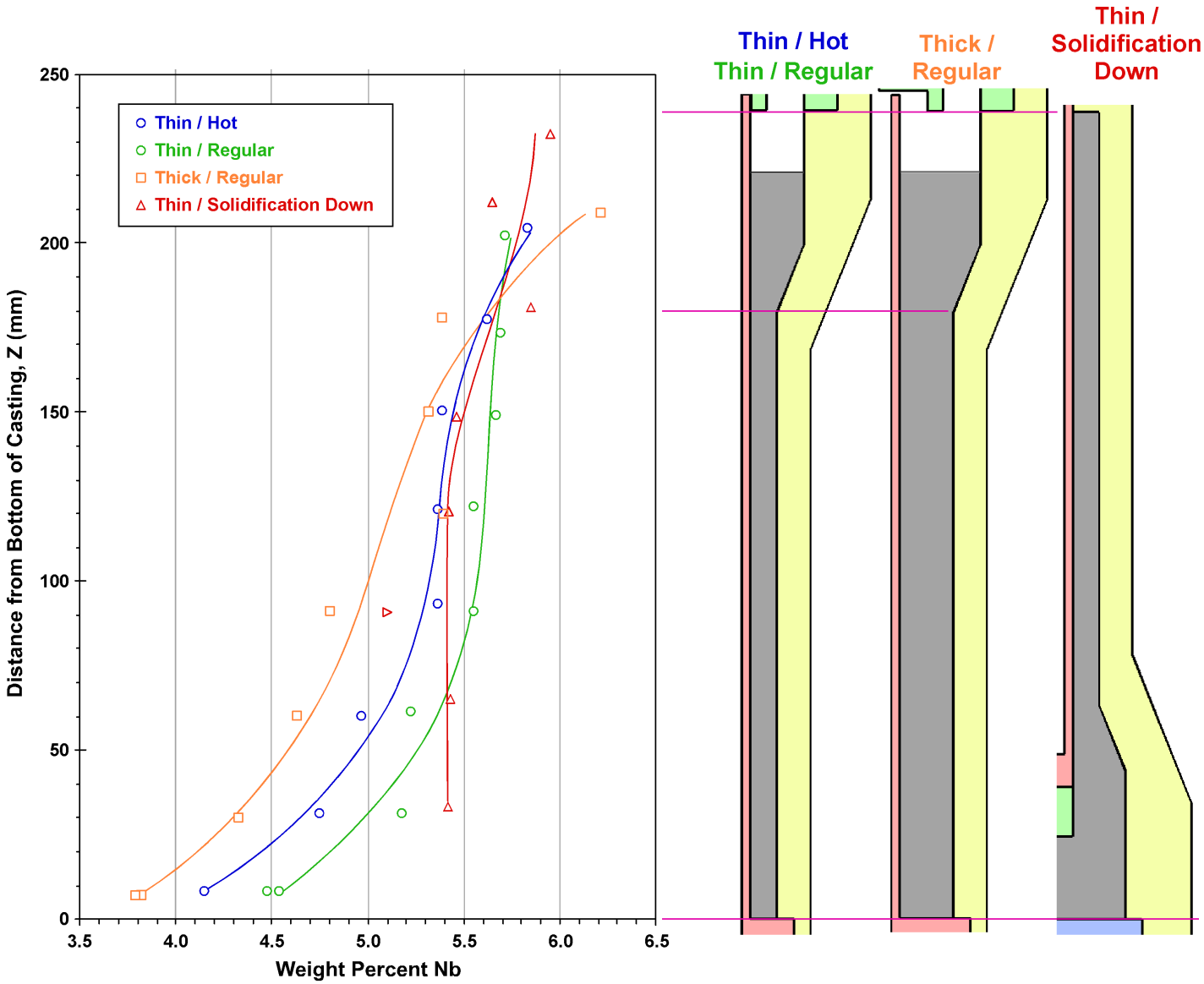

Fig. 20 Chemical analysis results as function of position plotted relative to the cross section of the 4 different castings.

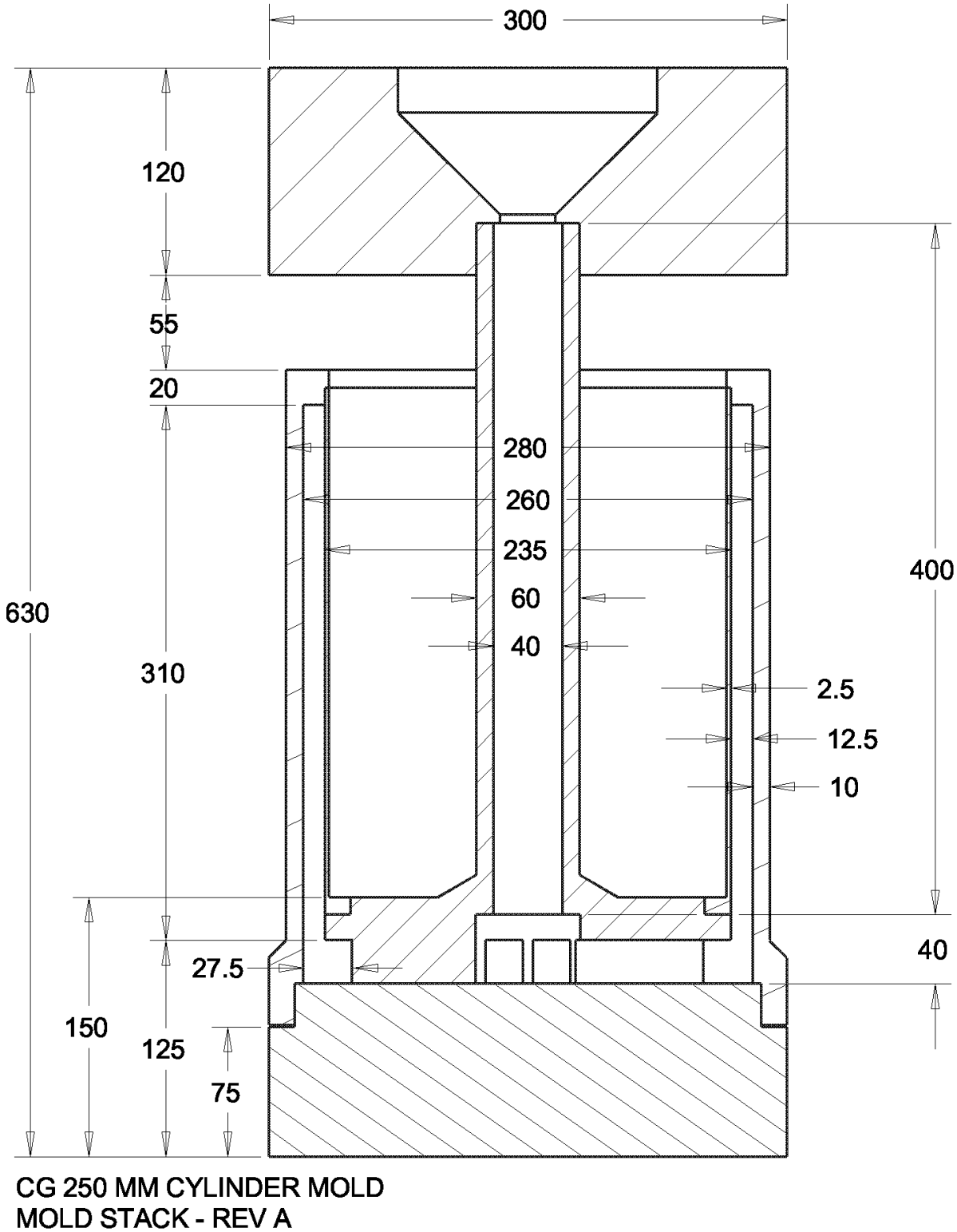

Fig. 21 Mold stack design for the larger 250 mm counter gravity mold. Dimensions are in millimeters.

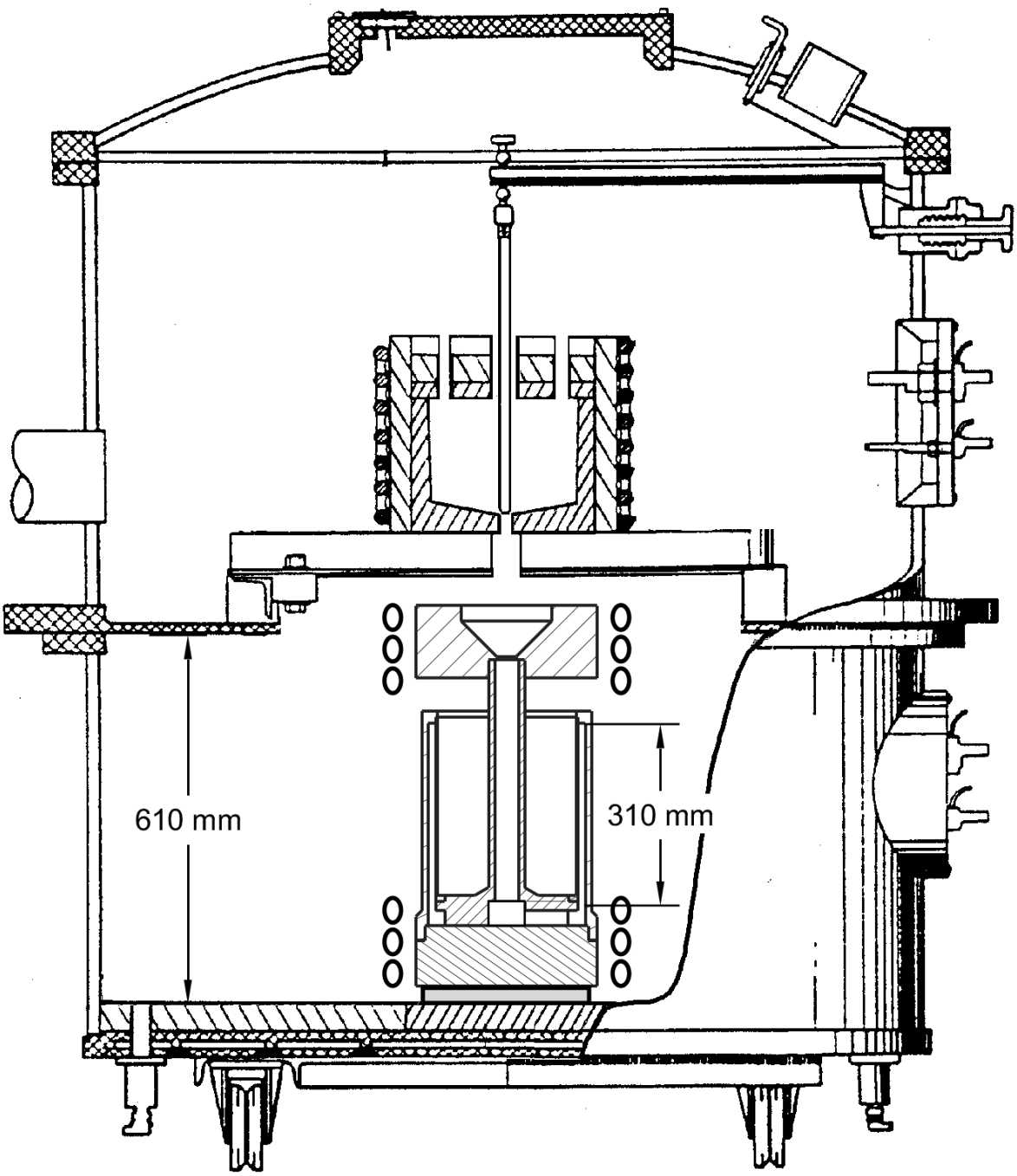

Fig. 22 Layout of counter gravity mold in furnace showing heating coils and crucible with stopper rod.

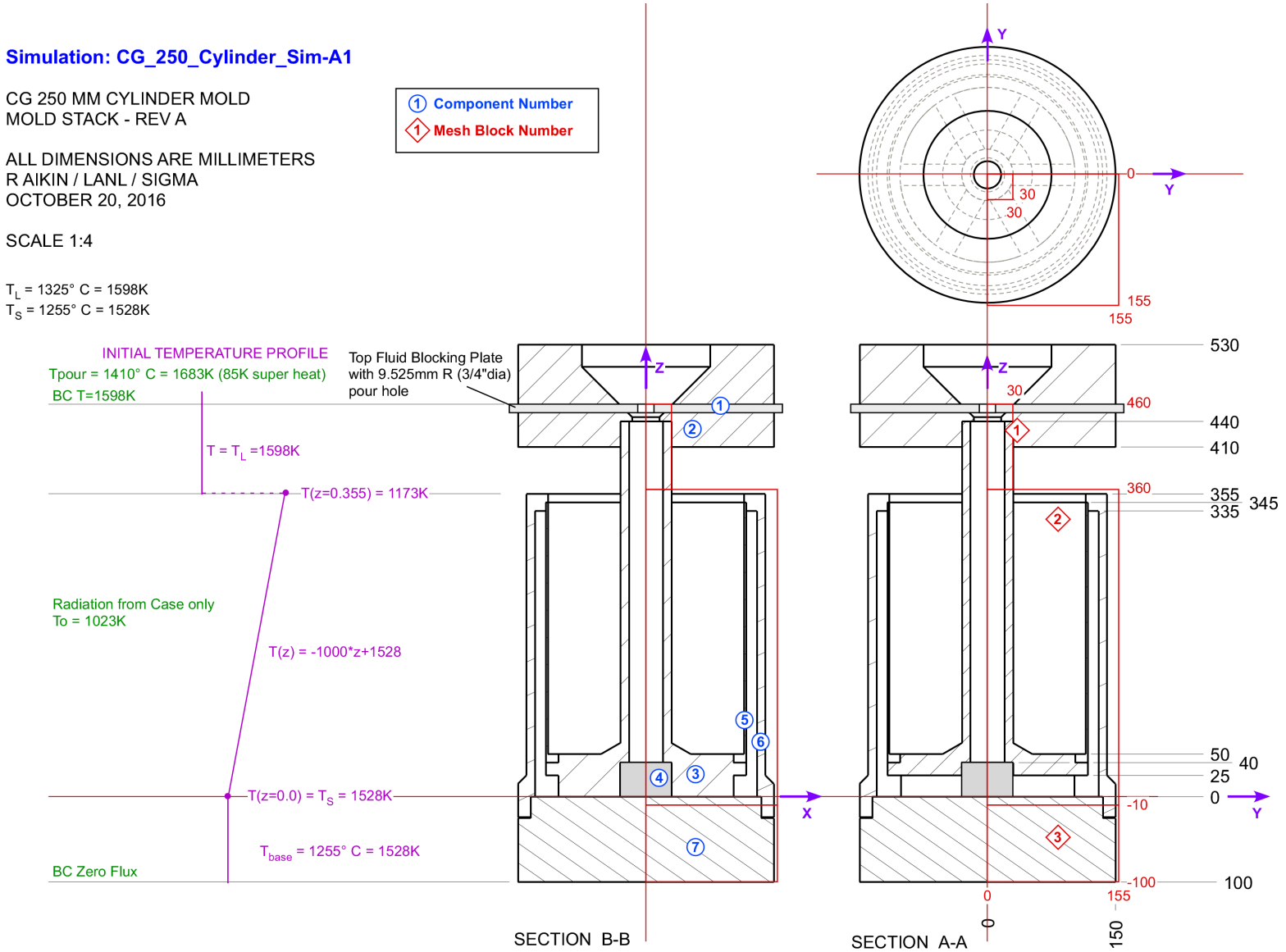

Fig. 23 Simulation setup showing the mold geometry, initial temperature distribution, and mesh/simulation boundaries.

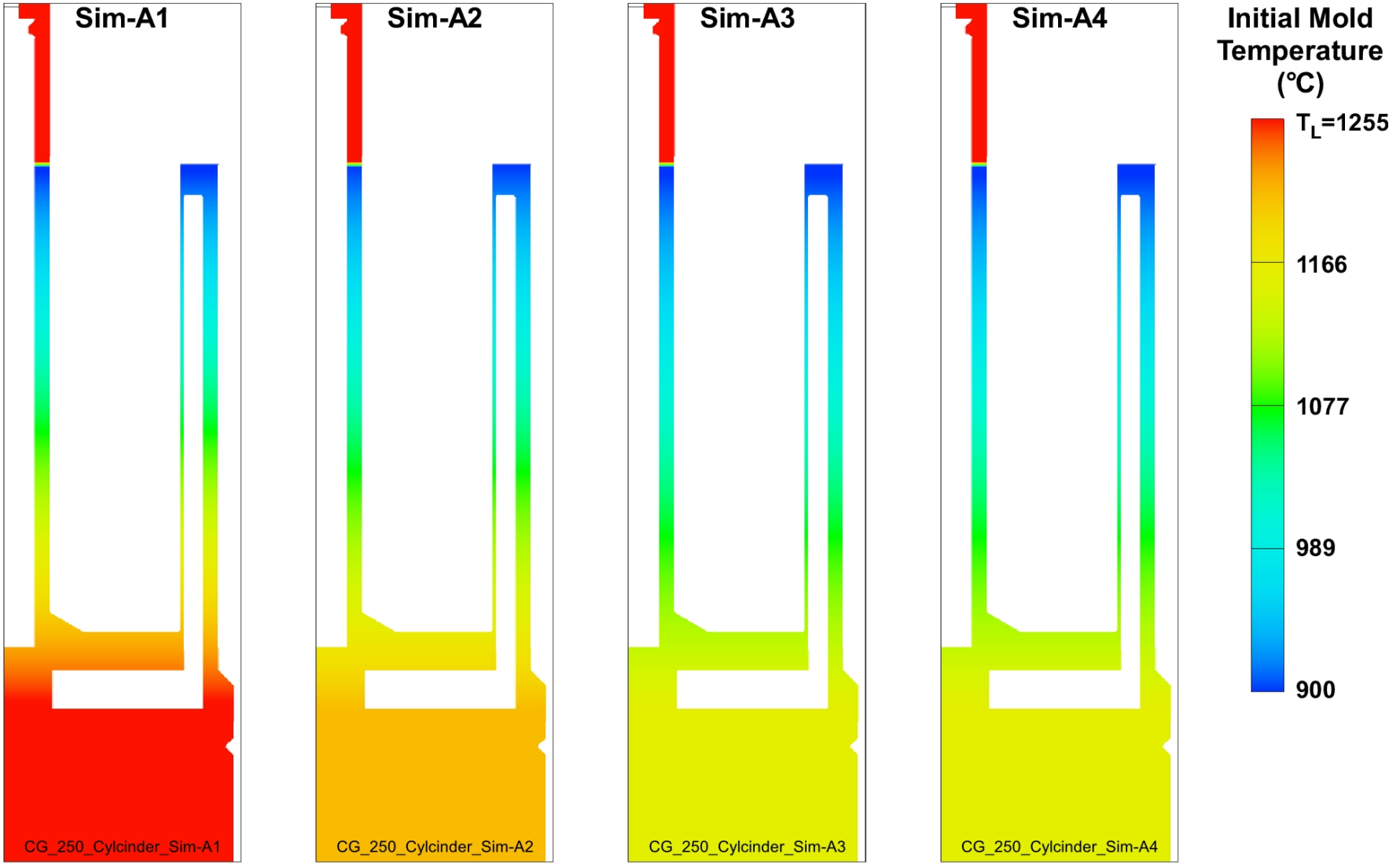

Fig. 24 Initial mold temperature distribution for simulations of filling and solidification of the revision A mold; simulations A1 though A4.

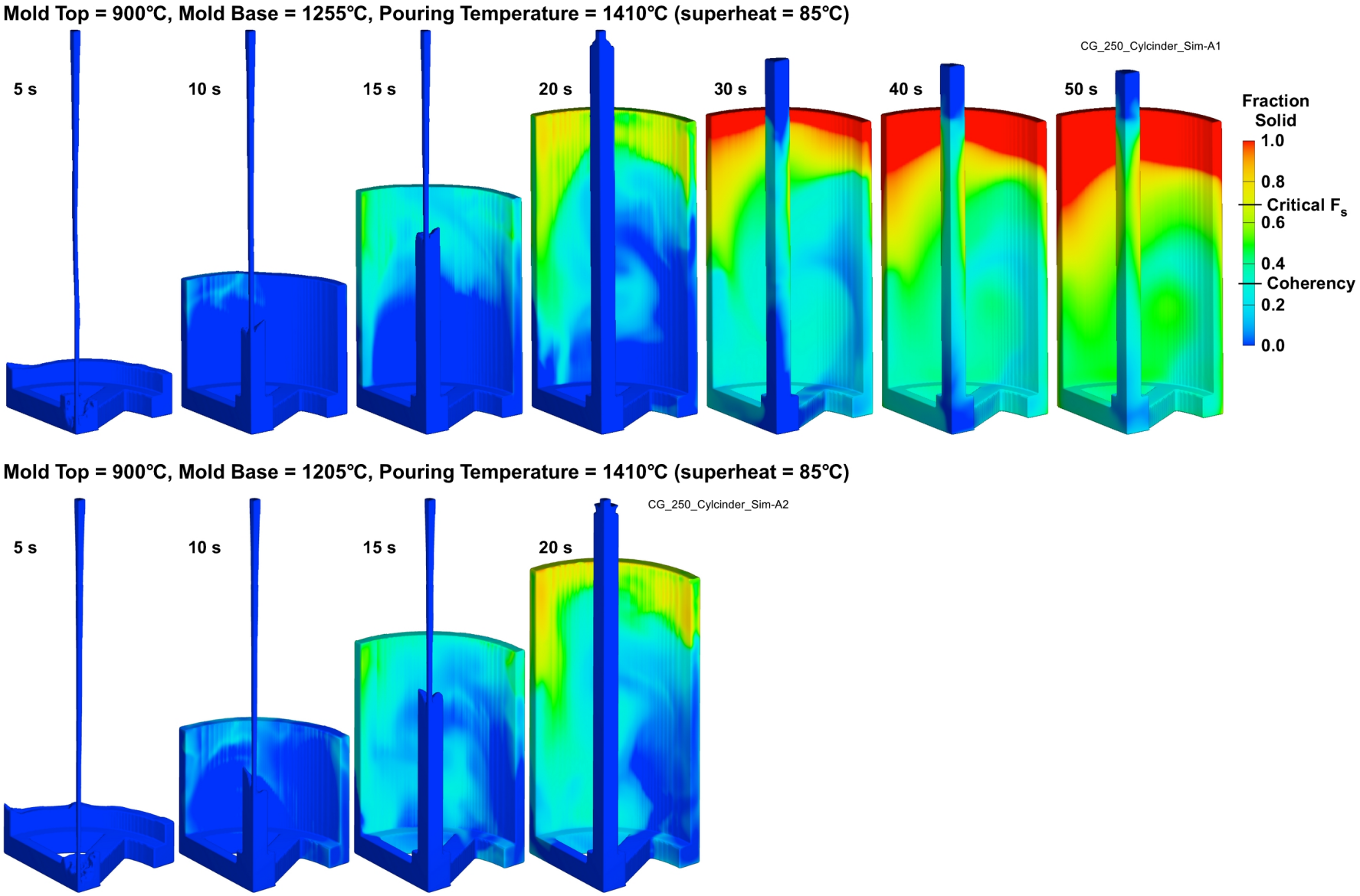

Fig. 25 Simulation results showing fraction solid as a function of time for simulations A1 (top) and A2 (bottom).

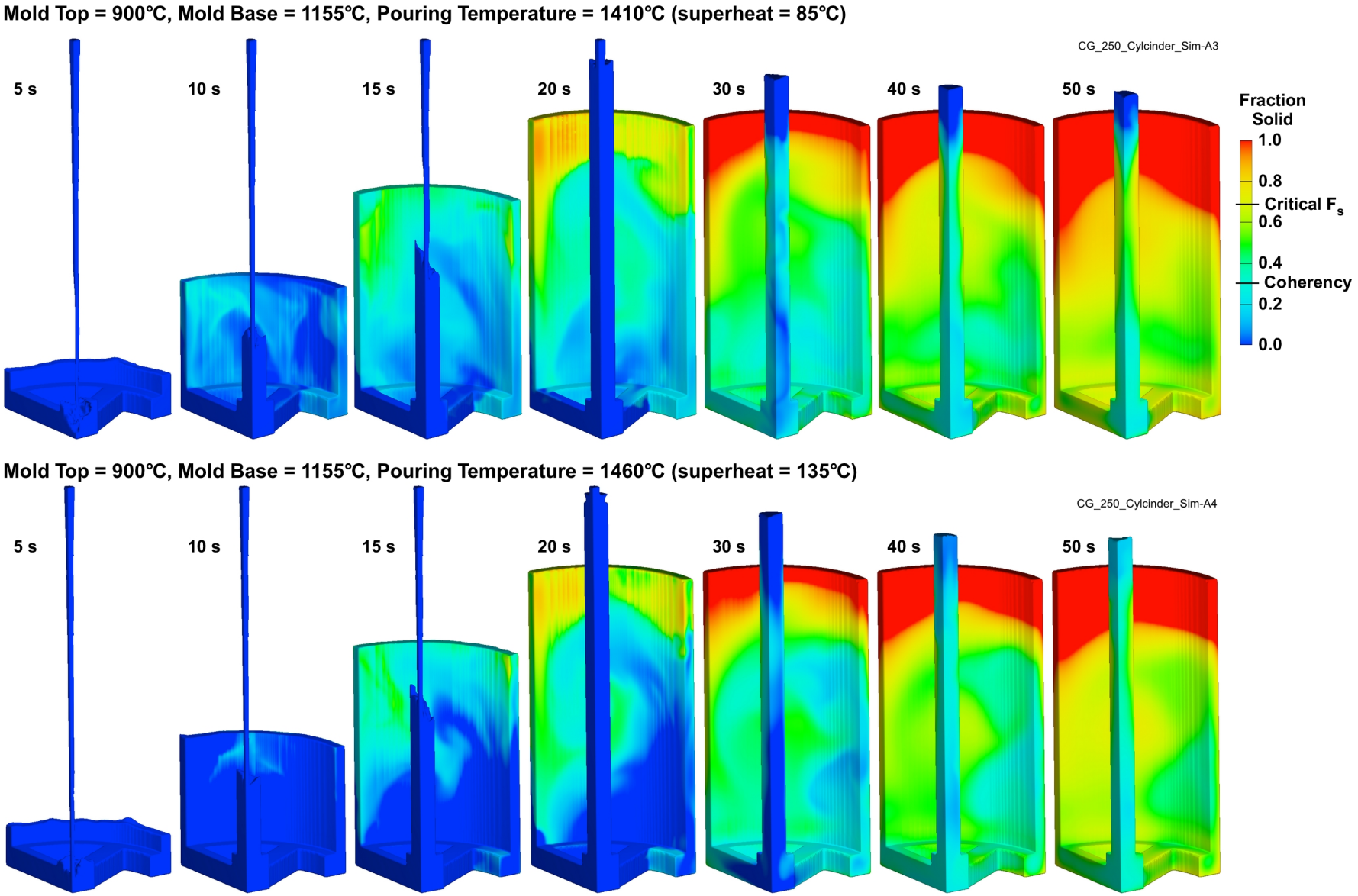

Fig. 26 Simulation results showing fraction solid as a function of time for simulations A3 (top) and A4 (bottom.

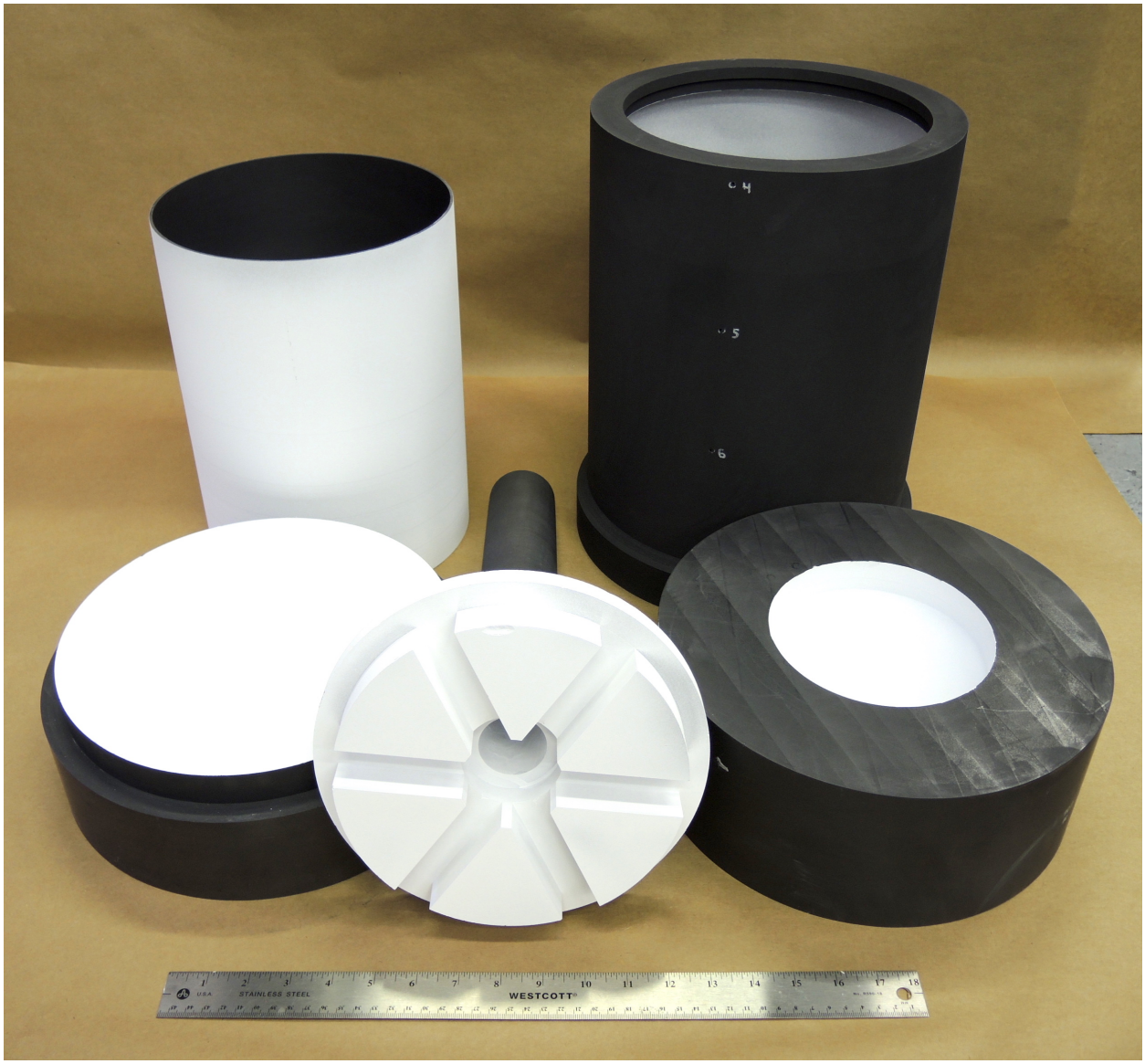

Fig. 27 Mold components of the 250 mm diameter counter gravity mold (revision A) prior to assembly. The white coating is the yittria mold coating.

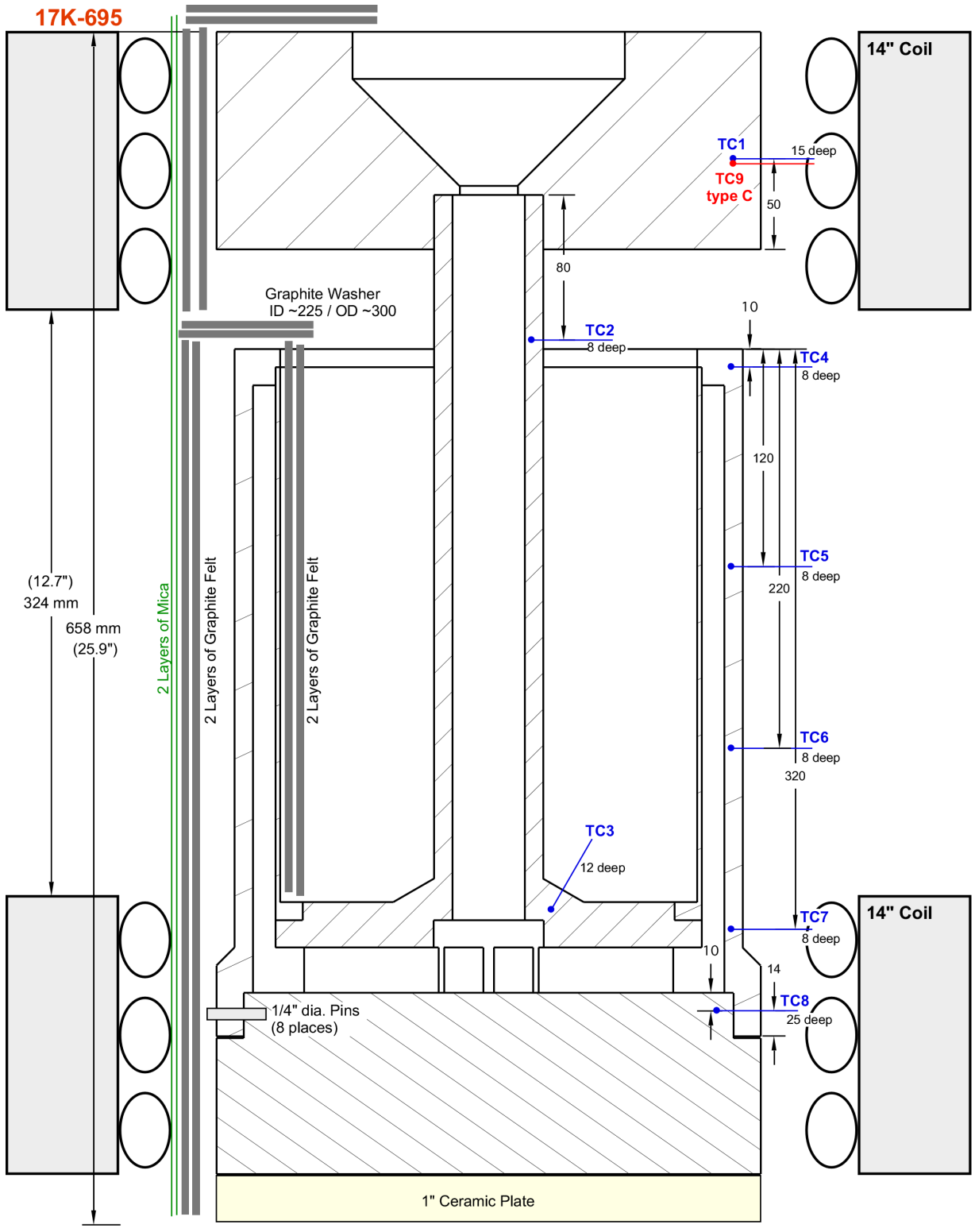

Fig. 28 Layout of thermocouples, induction coils, and insulation for casting 17K-695 with counter gravity 250 mm Cylinder mold revision A.

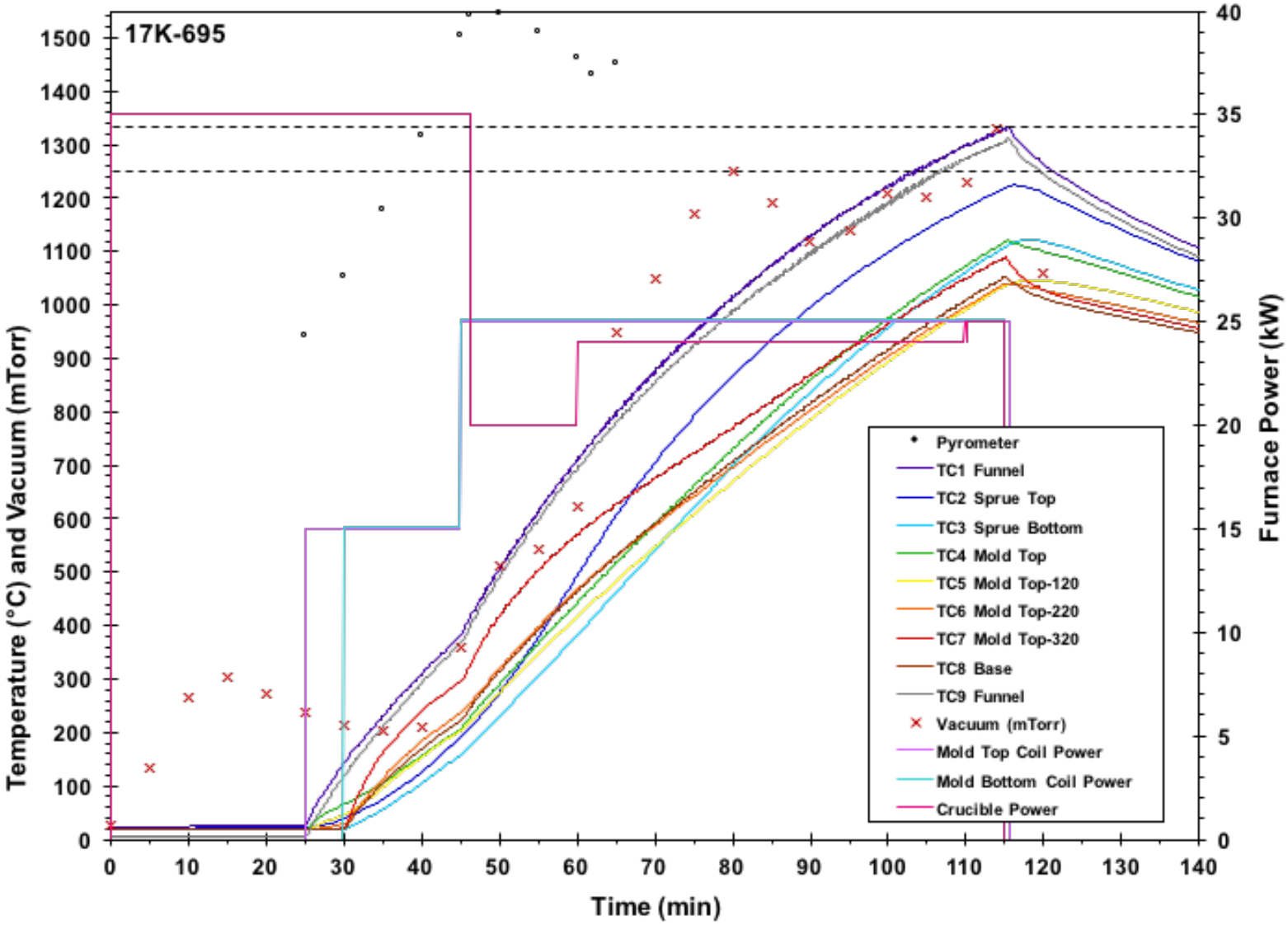

Fig. 29 Thermal history during heat up and casting of the revision A counter gravity 250 mm cylinder casting 17K-695.

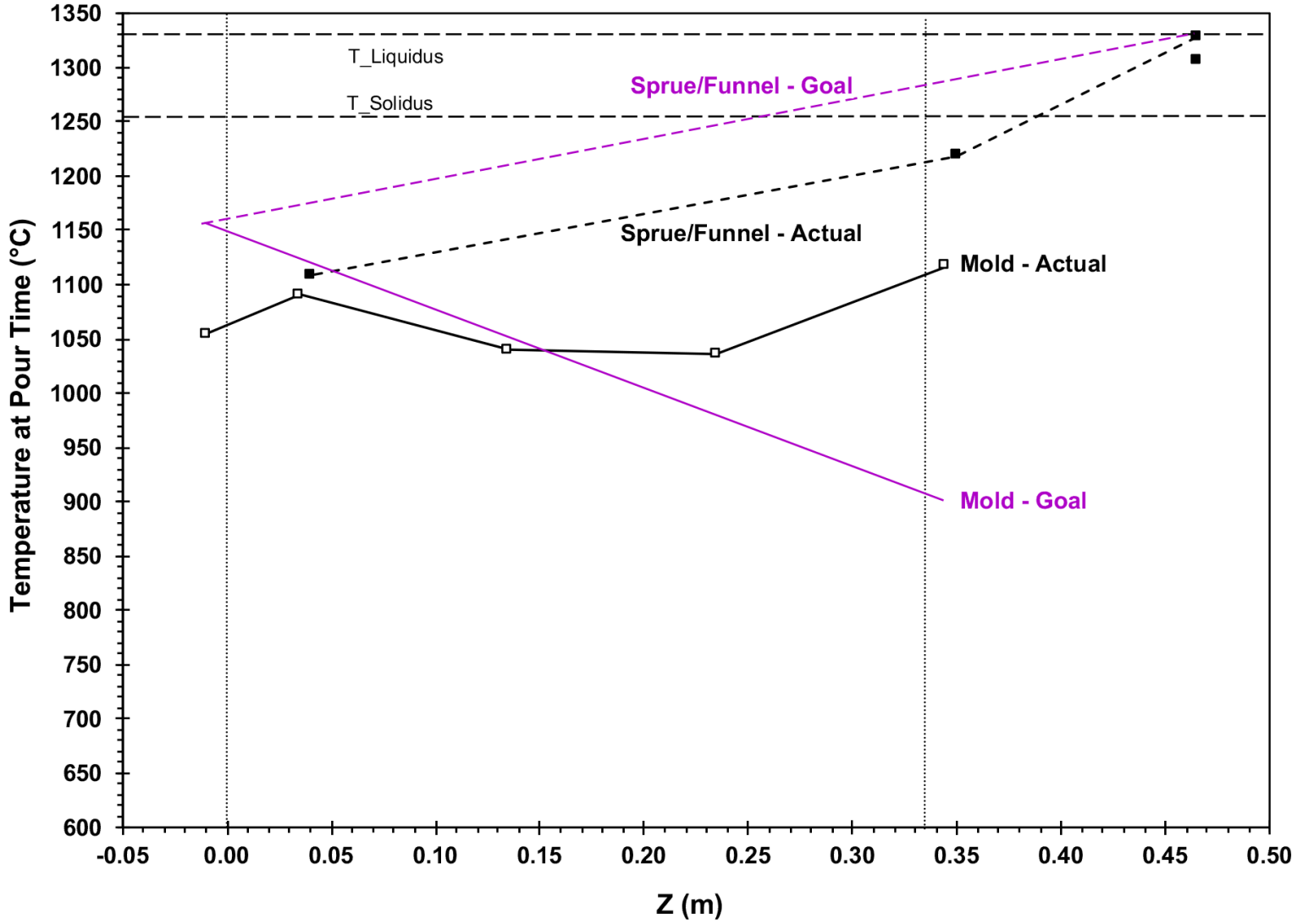

Fig. 30 Temperature as a function of position from the bottom of the casting for the 250 mm counter gravity cylinder casting 17K-695 at pour time. Black lines are actual temperature; purple lines are desired temperature.

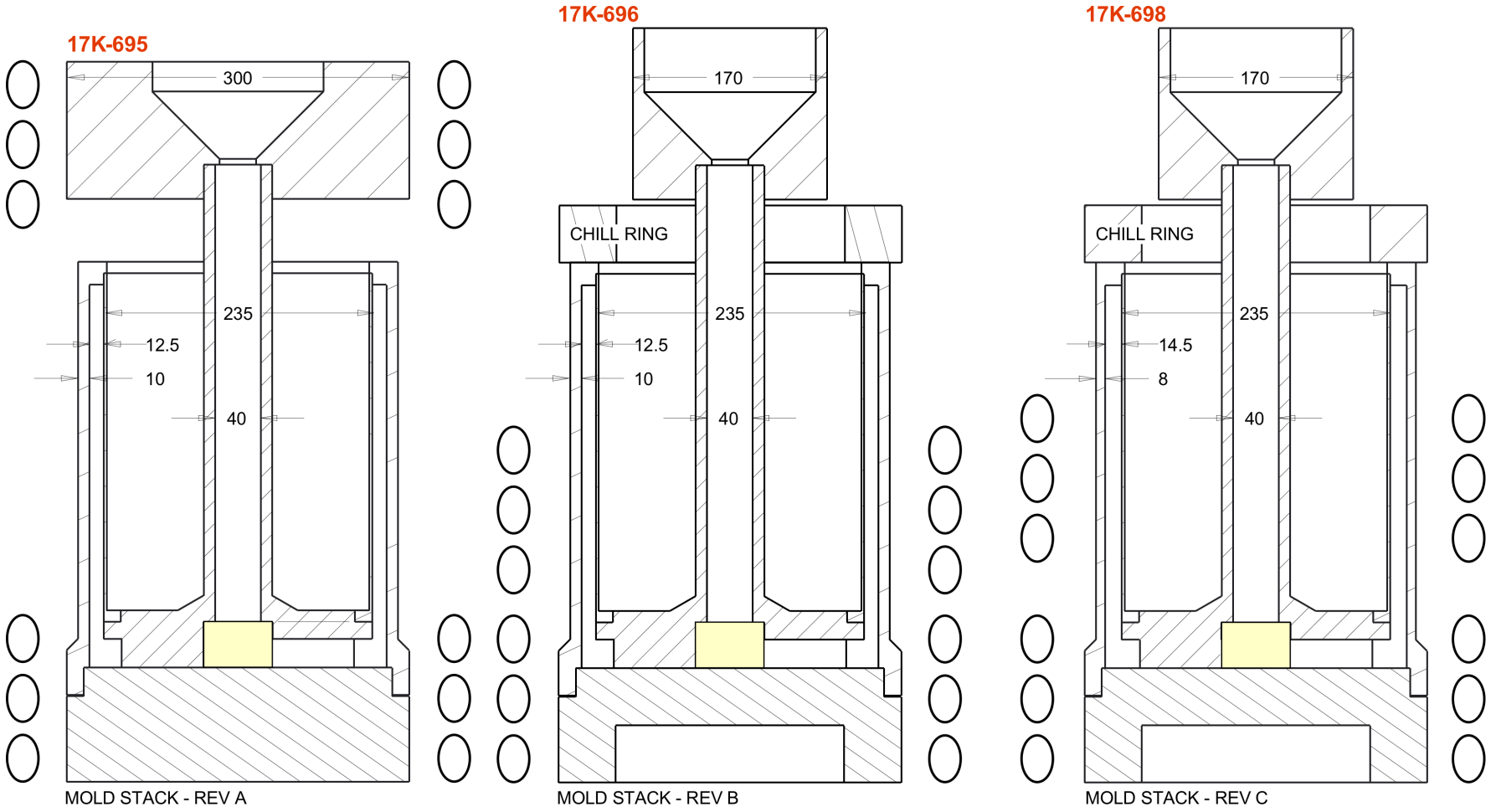

Fig. 31 Comparison of the three versions of the 250 mm diameter cylinder counter gravity mold cast.

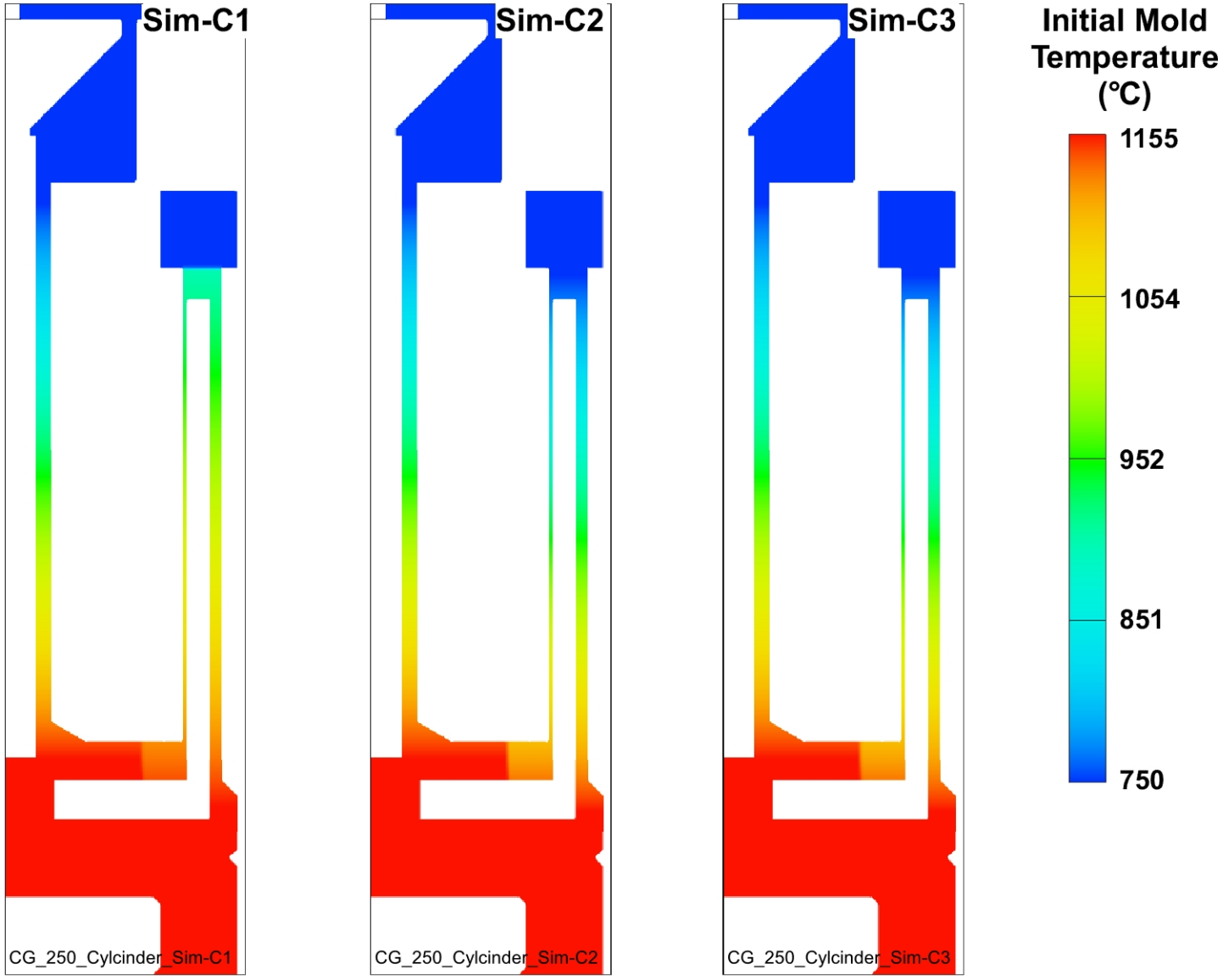

Fig. 32 Initial mold temperature distribution for simulations of filling and solidification of the revision C mold.

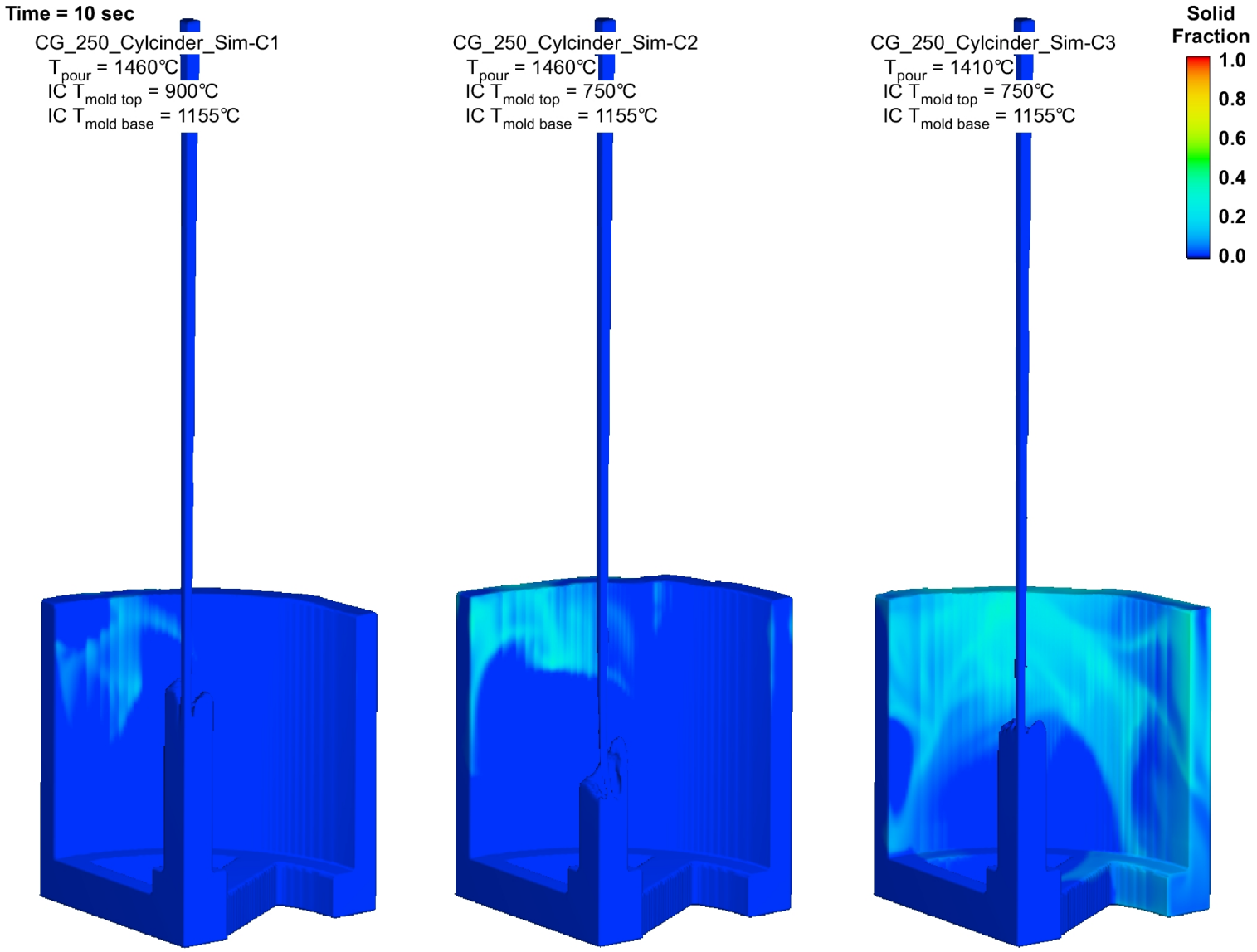

Fig. 33 Simulation results showing fraction solid at 10 seconds for the 3 initial conditions considered with revision C mold.

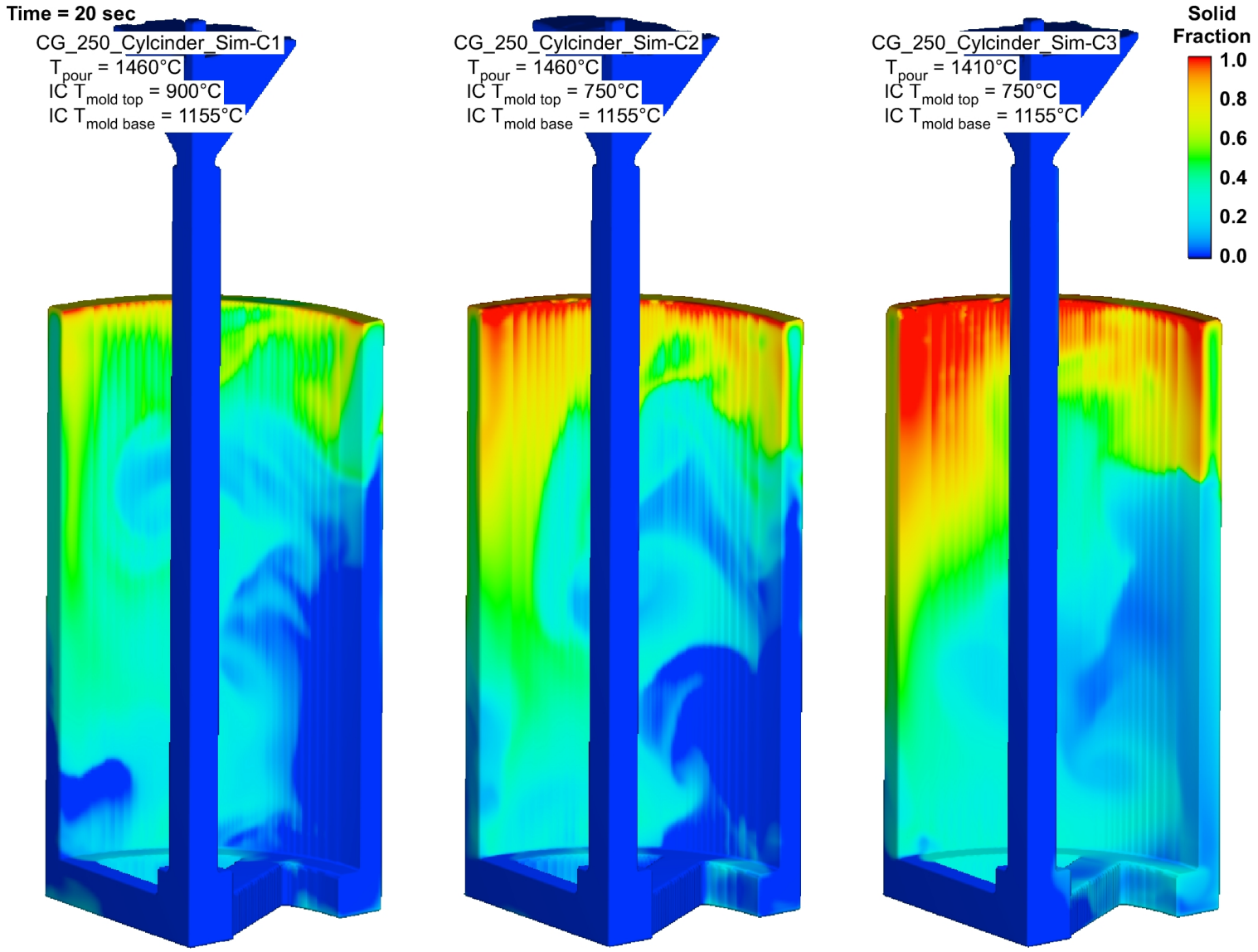

Fig. 34 Simulation results showing fraction solid at 20 seconds for the 3 initial conditions considered with revision C mold.

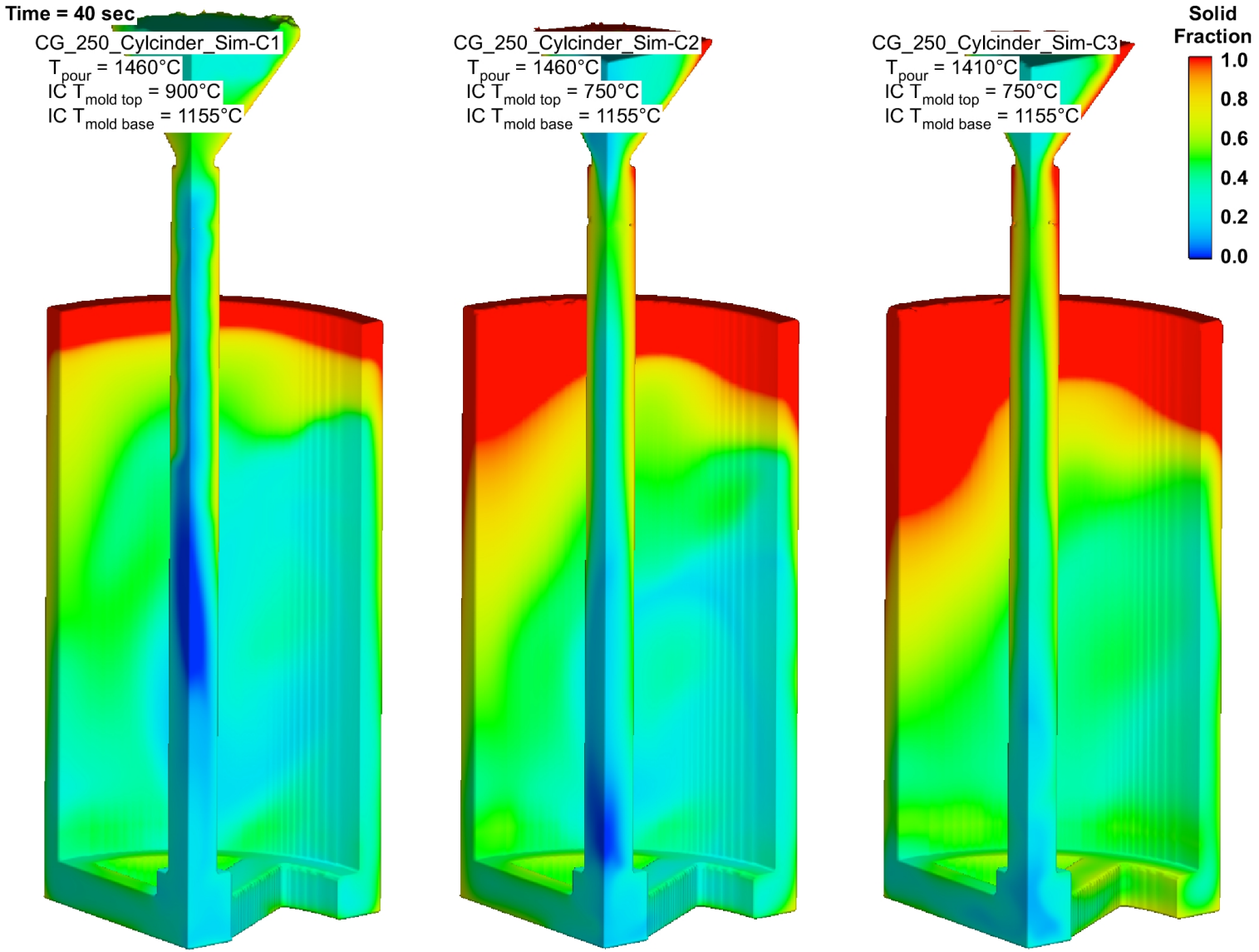

Fig. 35 Simulation results showing fraction solid at 40 seconds for the 3 initial conditions considered with revision C mold.

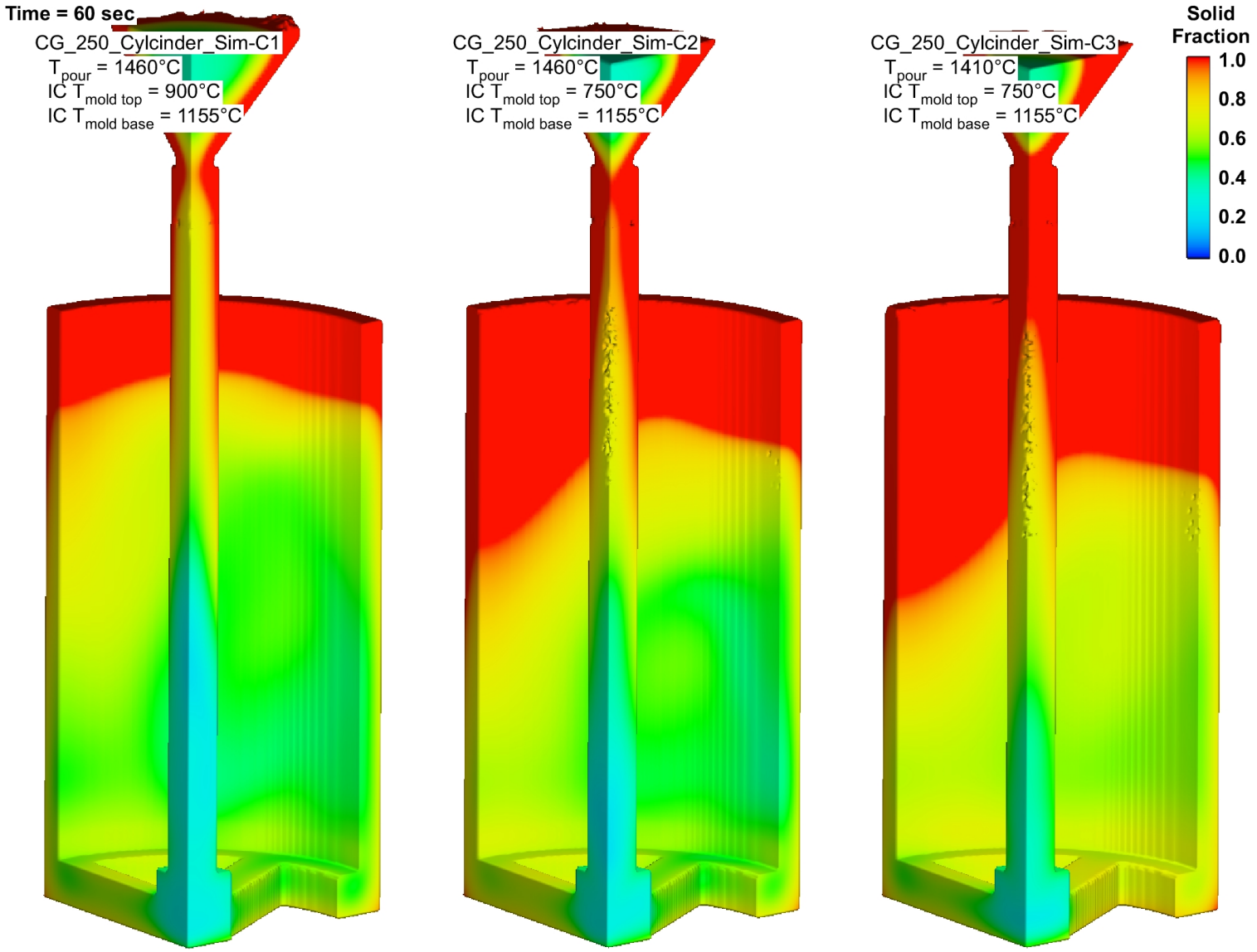

Fig. 36 Simulation results showing fraction solid at 60 seconds for the 3 initial conditions considered with revision C mold.

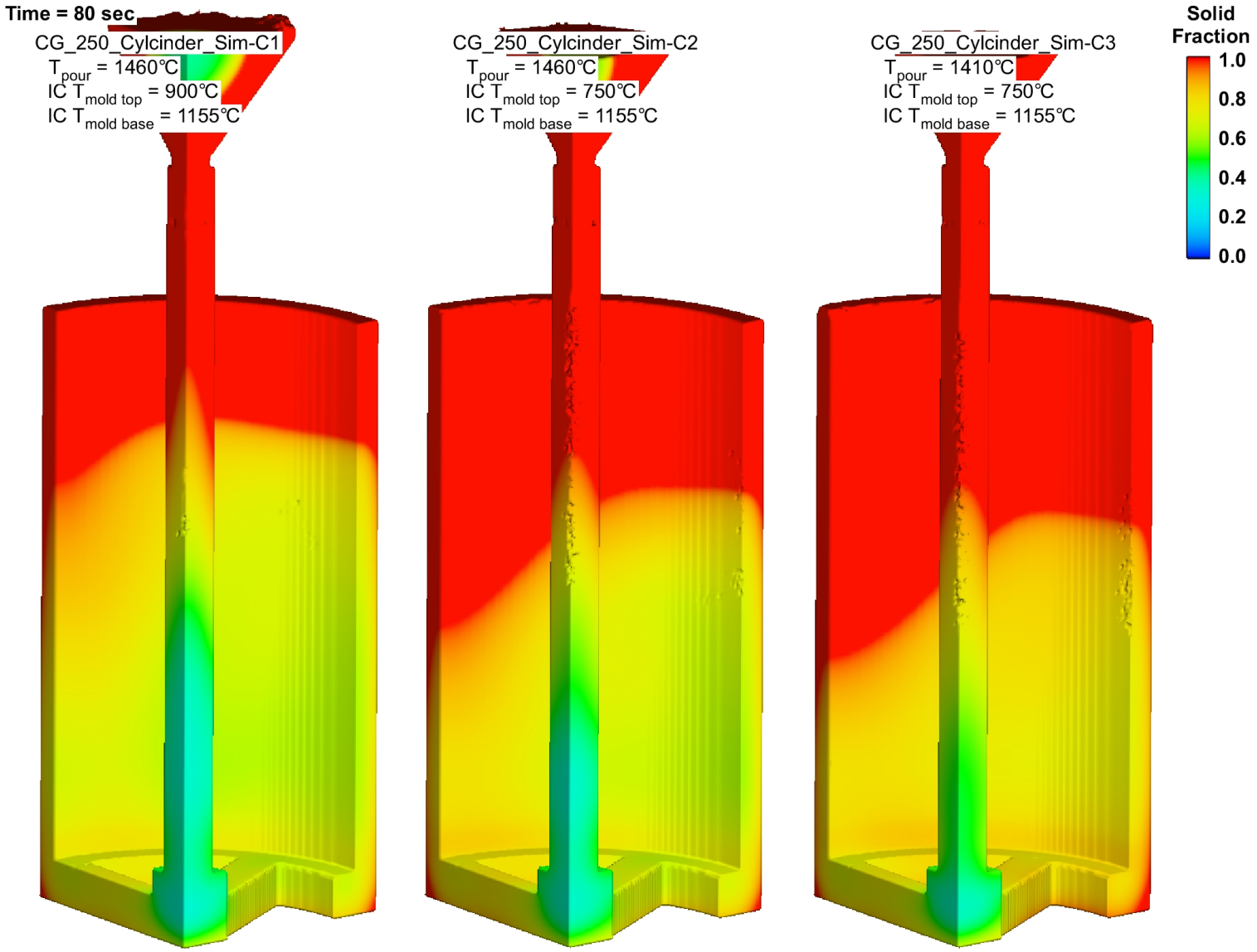

Fig. 37 Simulation results showing fraction solid at 80 seconds for the 3 initial conditions considered with revision C mold.

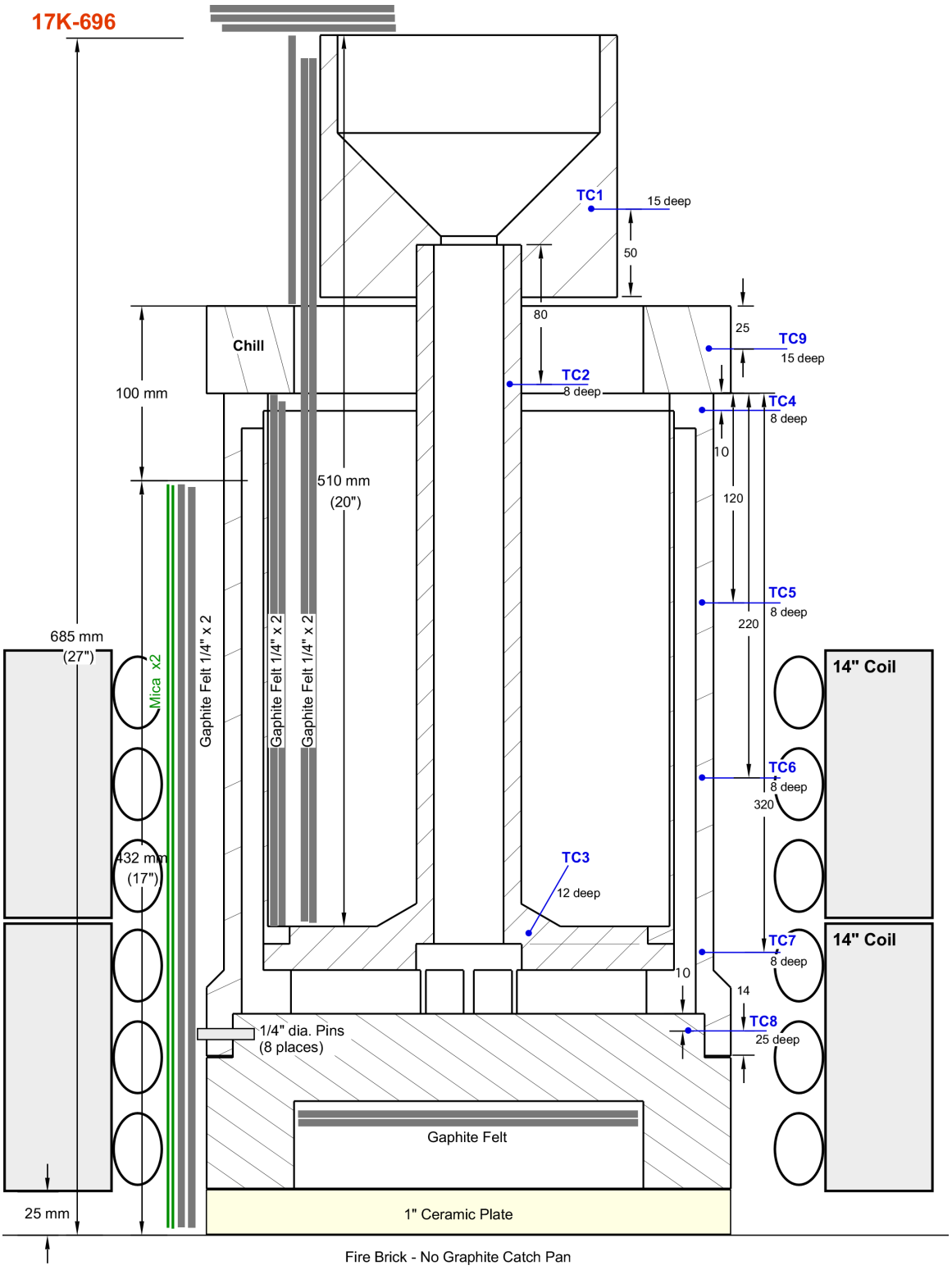

Fig. 38 Layout of thermocouples, induction coils, and insulation for casting 17K-696 with counter gravity 250 mm cylinder mold revision B.

Fig. 39 Counter gravity casting mold assembly prior to installation of the induction heating coils and insulation. The stainless steel sheathed type-K thermocouples are the silver wires. Blue painters tape keeps mold interior clean during assembly and is removed prior to casting 17K-696.

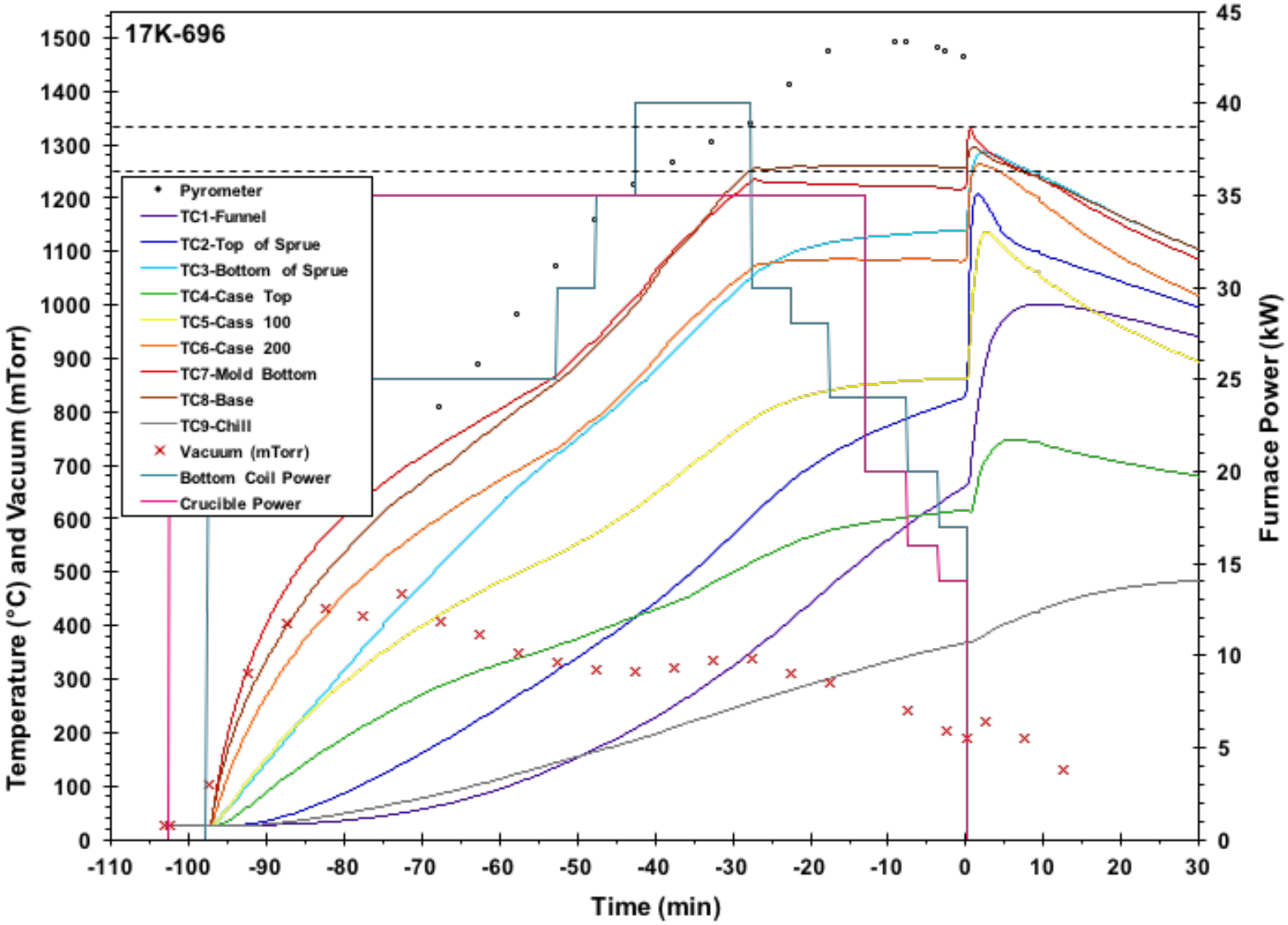

Fig. 40 Thermal history during heat up and casting of the revision B counter gravity 250 mm cylinder casting 17K-696.

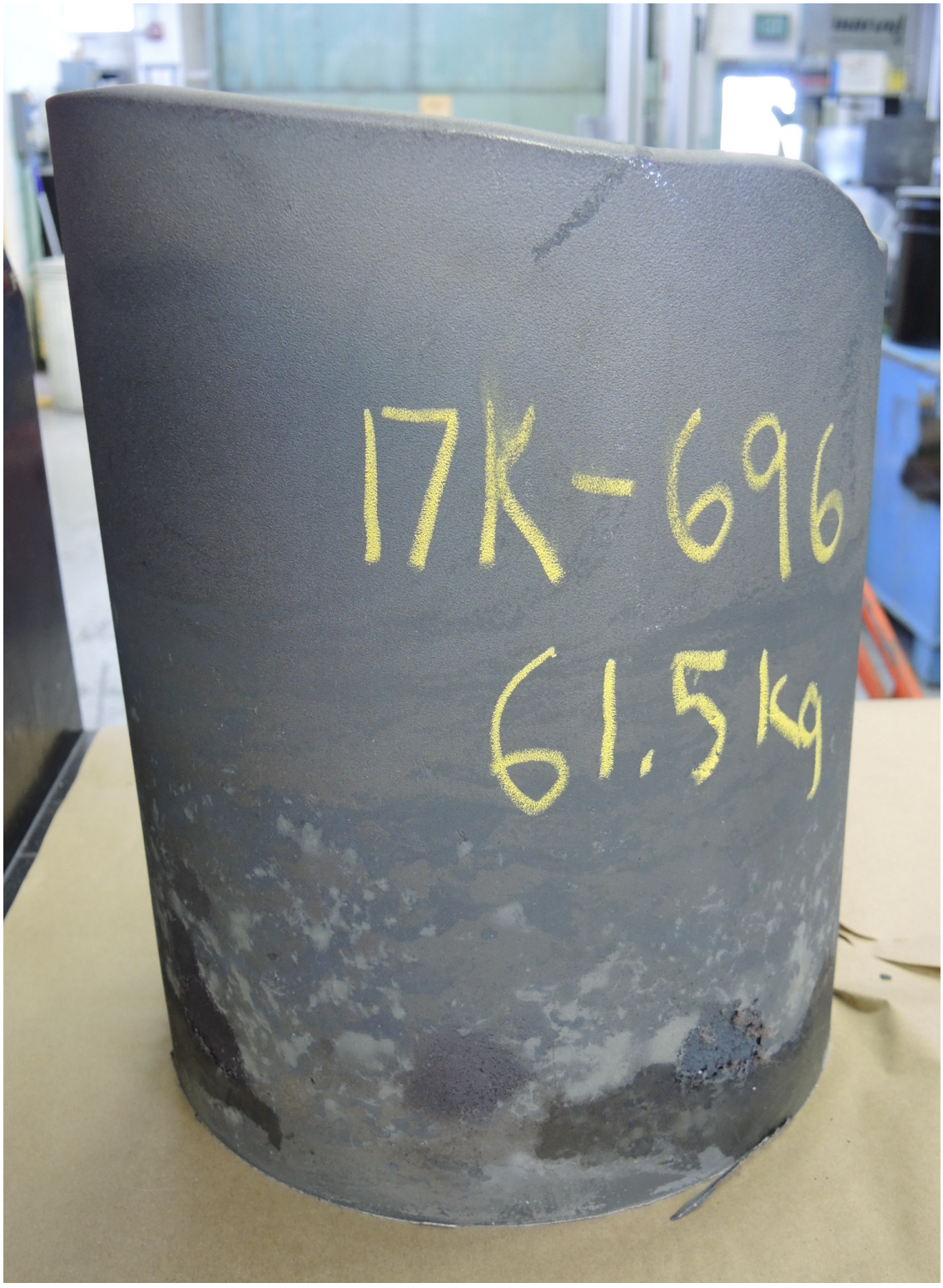

Fig. 41 Resulting casting 17K-696 from counter gravity 250 mm with revision B mold.

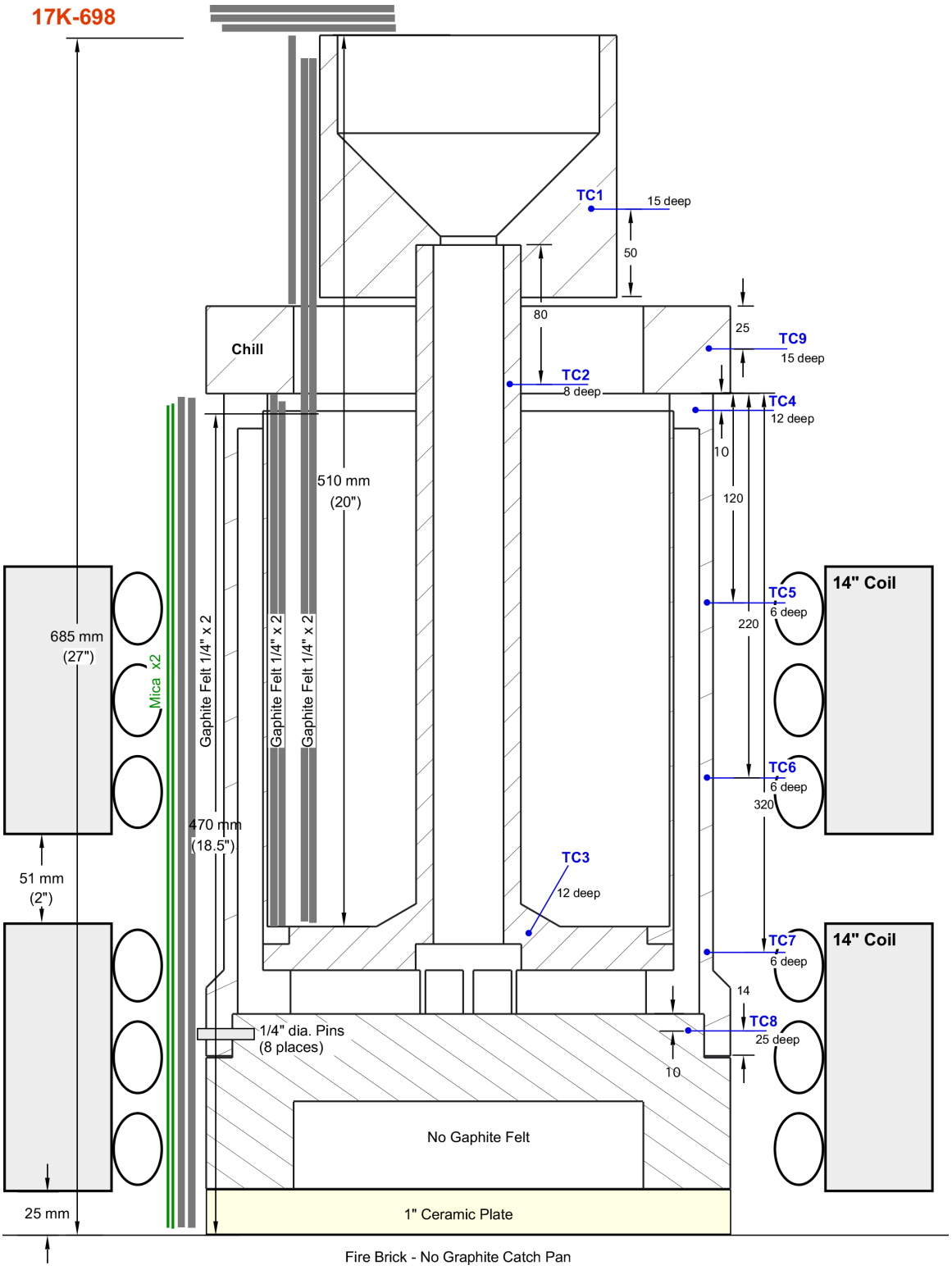

Fig. 42 Layout of thermocouples, induction coils, and insulation for casting 17K-698 with counter gravity 250 mm cylinder mold revision C.

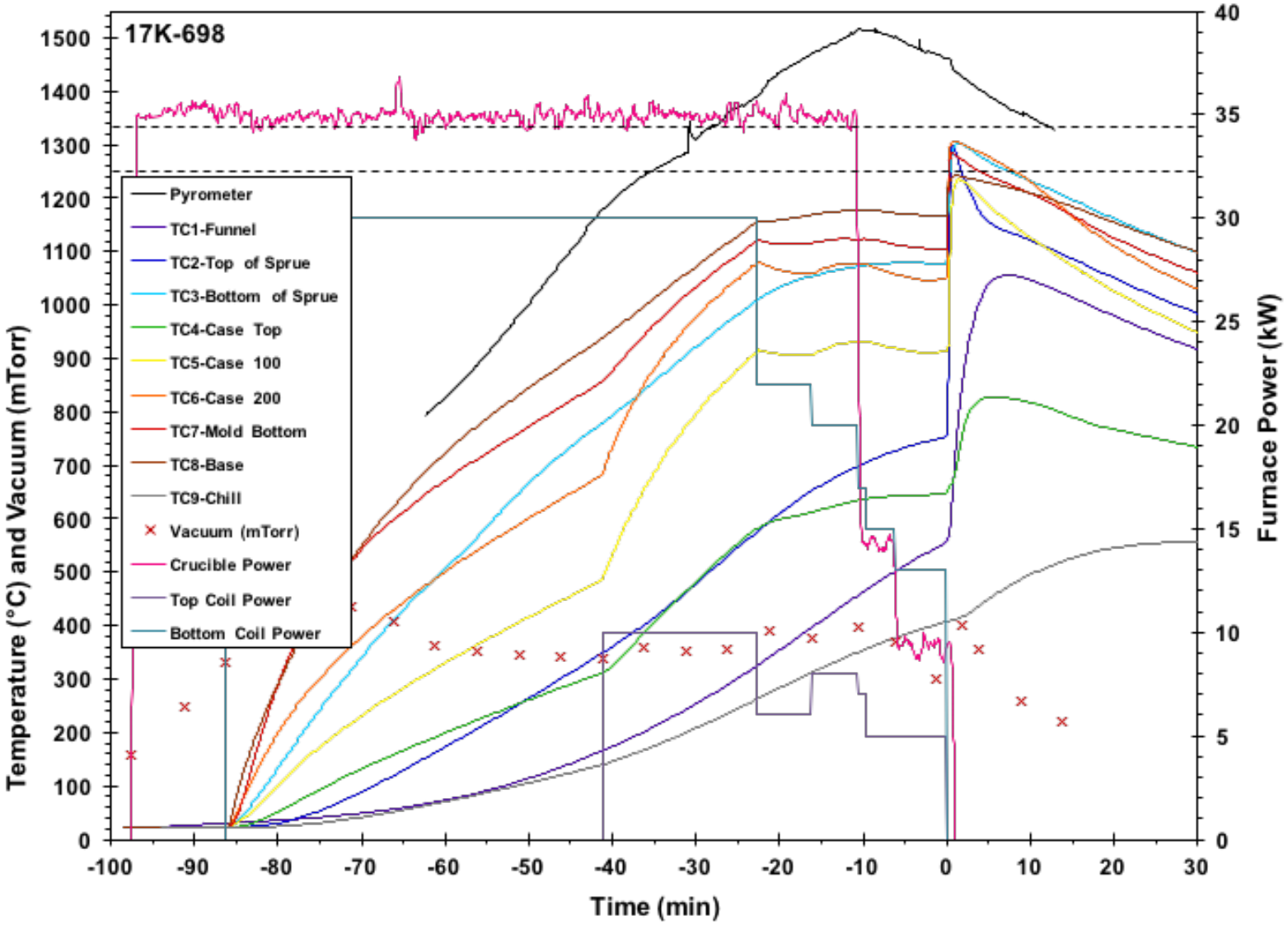

Fig. 43 Thermal history during heat up and casting of the revision C counter gravity 250 mm cylinder casting 17K-698.

Fig. 44 Resulting casting 17K-698 from counter gravity 250 mm with revision C mold. Casting is show upside down with bottom of casting at top of photo.

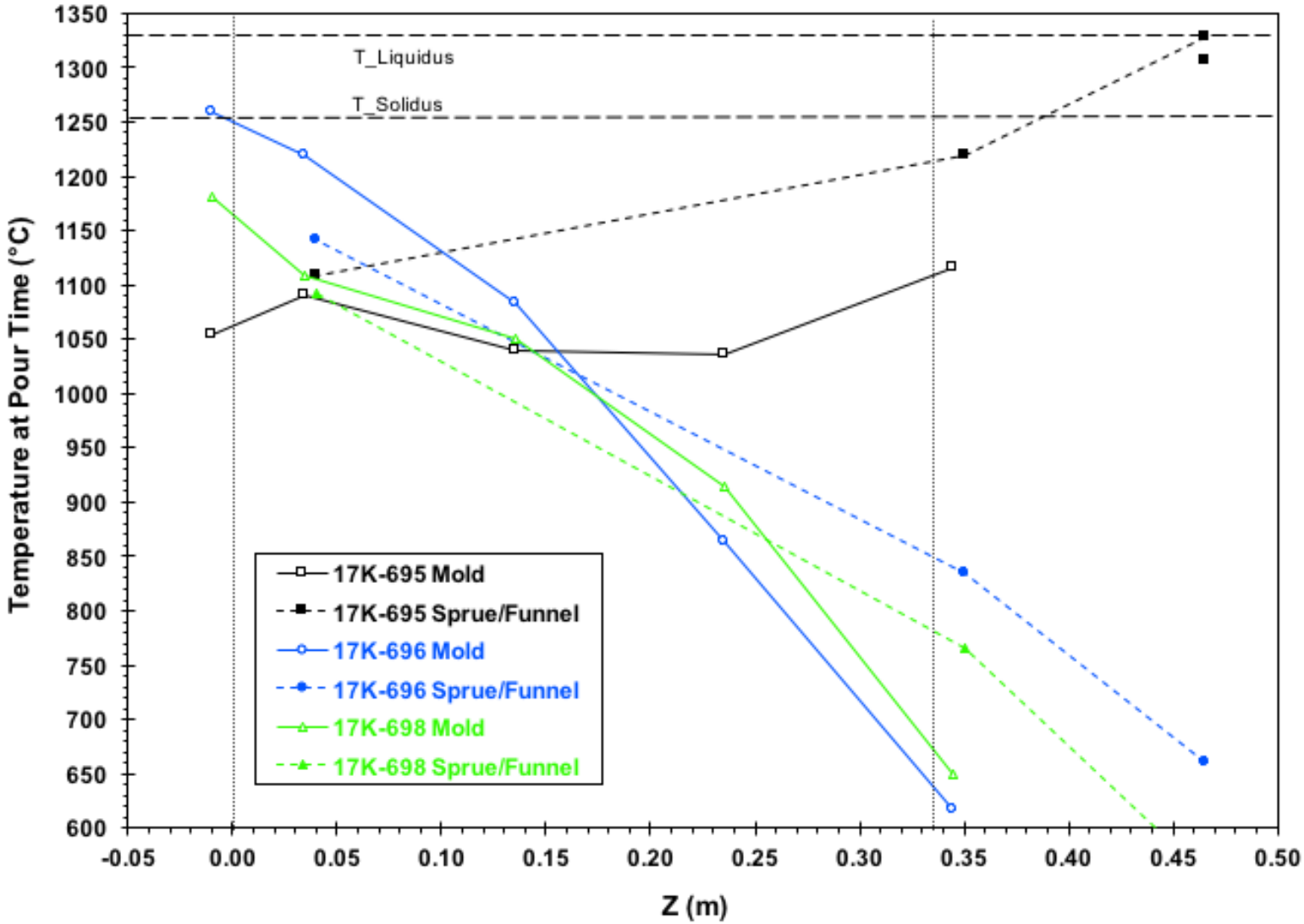

Fig. 45 Temperature as a function of position from the bottom of the casting for the counter gravity 250 mm cylinder castings at pour time.

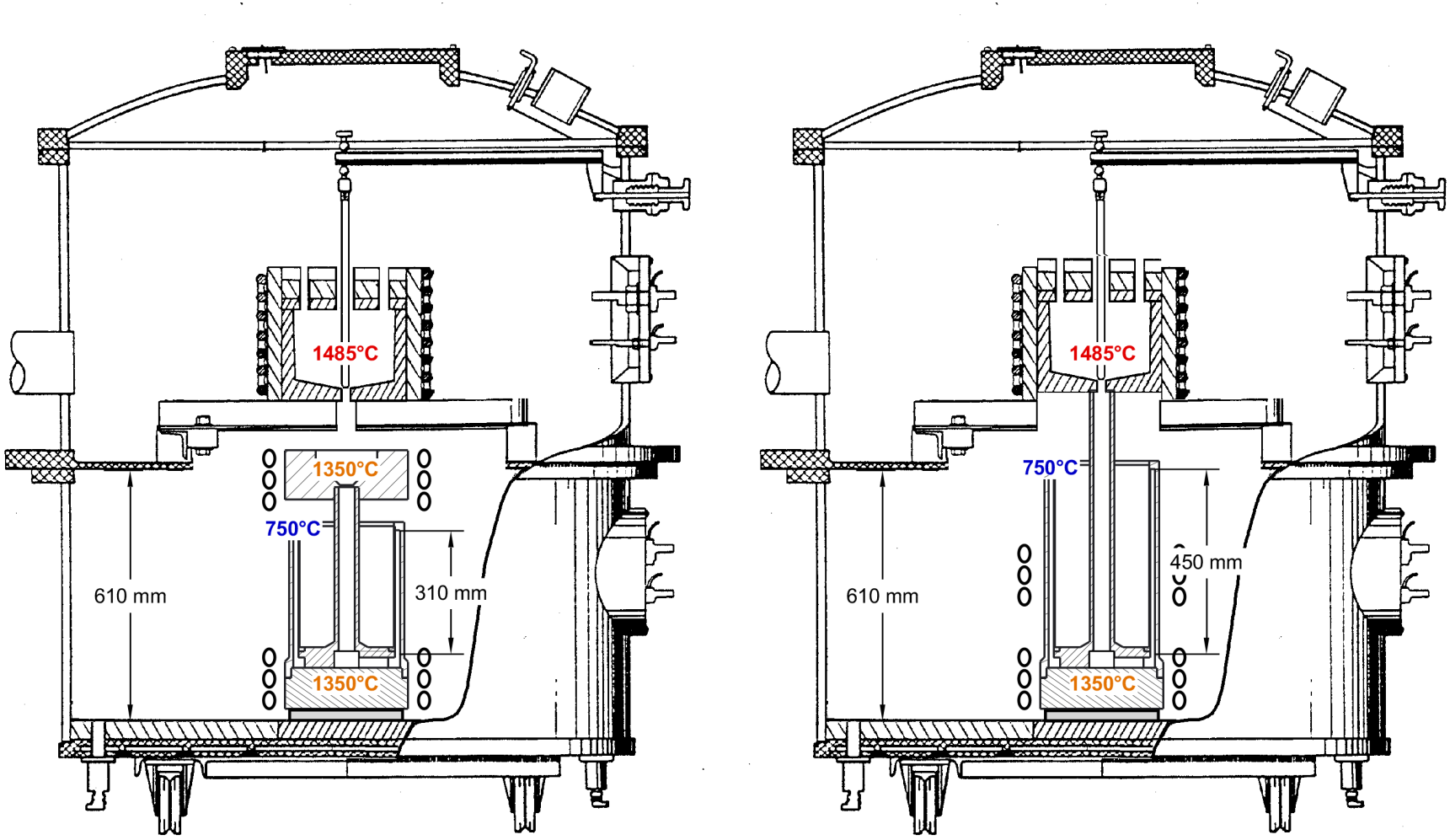

Fig. 46 Comparison of mold stack in furnace with desired initial temperature distribution: current configuration on left and future funnel less approach on right.